PGR5 is needed for redox-dependent regulation of ATP synthase both in chloroplasts and in cyanobacteria

Lauri Nikkanen[1]*, Laura T. Wey[1], Russell Woodford[2], Henna Mustila[1], Darius Kosmützky[3], Maria Ermakova[2], Eevi Rintamäki[1], and Yagut Allahverdiyeva[1]*

[1]Molecular Plant Biology, Department of Life Technologies, University of Turku, Finland

[2]School of Biological Sciences, Monash University, Australia

[3]Department of Biochemistry, University of Cambridge, United Kingdom

*Co-corresponding authors

Authors for Correspondence:

Lauri Nikkanen, Molecular Plant Biology, Department of Life Technologies, University of Turku, Turku 11 FI- 20014, Finland. E-mail: lenikk@utu.fi

Yagut Allahverdiyeva, Molecular Plant Biology, Department of Life Technologies, University of Turku, Turku 11 FI-20014, Finland. E-mail: allahve@utu.fi

ORCID identifiers:

Lauri Nikkanen: 0000-0002-7192-9322

Laura T. Wey: 0000-0003-2345-0699

Russell Woodford: 0000-0002-6766-2274

Henna Mustila: 0000-0002-1939-7197

Darius Kosmützky: 0000-0002-6678-7550

Maria Ermakova: 0000-0001-8466-4186

Eevi Rintamäki: 0000-0002-1353-3995

Yagut Allahverdiyeva: 0000-0002-9262-1757

Running title: PGR5-dependent regulation of ATP synthase

Number of Figures: 8

Supplementary Data: 18 Figures and 10 Tables

Word count: 9598

Highlight

PGR5 is involved in regulation of ATP synthase in fluctuating light conditions across photosynthetic organisms in a manner that depends on the thiol redox state of the chloroplast or cell.

ABSTRACT

The regulation of proton motive force (*pmf*) via ATP synthase activity is a critical mechanism by which photosynthetic organisms maintain redox homeostasis and activate photoprotective responses under fluctuating light conditions. Here, we used time-resolved electrochromic shift (ECS) measurements to investigate *pmf* dynamics across a range of photosynthetic organisms. Our results reveal that ATP synthase is dynamically regulated during light fluctuations, but in *Arabidopsis thaliana* could this regulation could not be explained by the known light-induced reduction of the CF□γ subunit, suggesting alternative control mechanisms. The PROTON GRADIENT REGULATION 5 (PGR5) protein, previously proposed to facilitate cyclic electron transport (CET), also has a potential role in ATP synthase regulation. The physiological role of cyanobacterial Pgr5 has remained elusive. We characterised a Δ*pgr5* mutant of *Synechocystis* sp. PCC 6803 and investigated *pmf* dynamics in *pgr5* mutants of *Chlamydomonas reinhardtii*, Arabidopsis, and the C4 grass *Setaria viridis*. While PGR5 was not required for CET in *Synechocystis*, it was needed for downregulating ATP synthase under high irradiance in all tested organisms via a thiol redox state dependent mechanism. Furthermore, interaction between AtPGR5 and AtCF□γ suggests that PGR5 functions as a conserved inhibitor of ATP synthase under high light, contributing to *pmf* retention and photoprotection.

KEYWORDS: Photosynthesis, ATP synthase, proton motive force, chloroplast, cyanobacteria, Arabidopsis, electrochromic shift

INTRODUCTION

Oxygenic photosynthesis by plants, algae, and cyanobacteria uses light energy to drive oxidation of water to produce ATP and NADPH for CO_2 fixation and other cellular processes. In their natural habitats, oxygenic photosynthetic organisms undergo constant fluctuation of irradiance. Mechanisms to adjust the redox homeostasis in chloroplasts and cyanobacterial cells have evolved to prevent energy-consuming futile reactions and damage to the photosynthetic machinery and other biomolecules via generation of reactive oxygen species (ROS) by the photosynthetic apparatus. ROS can be generated as a result of excitation imbalance between the photosystems, or when electron transport rate exceeds the sink capacity of the reactions downstream of the photosynthetic electron transport chain (PETC). Resulting accumulation of reduced electron carriers in the PETC triggers charge recombination reactions within the photosystems and direct reduction of O_2, generating highly reactive ROS such as superoxide ($O_2^{\bullet-}$) and hydrogen peroxide (H_2O_2) at PSI and singlet oxygen ($^1O_2$) primarily at PSII (Foyer & Hanke, 2022). PSI and its iron sulphur clusters are particularly vulnerable to over-reduction-induced damage, and plants, algae, and cyanobacteria invest heavily in their protection (Tiwari *et al.*, 2016, 2024). These protective mechanisms involve cyclic electron transport around PSI (CET), redistribution of excitation energy between the photosystems via state transitions, non-photochemical quenching (NPQ), and inhibition of PQH_2 oxidation at the cytochrome b_6f complex, known as photosynthetic control (Tikkanen & Aro, 2014; Shimakawa *et al.*, 2016; Nikkanen *et al.*, 2021; Eckardt *et al.*, 2024; Degen & Johnson, 2024). Additionally, in photosynthetic organisms apart from angiosperms, flavodiiron proteins provide a photoprotective electron sink on the acceptor side of PSI by catalysing controlled reduction of O_2 to water (the Mehler-like reaction) (Allahverdiyeva *et al.*, 2013; Ilik *et al.*, 2017).

As photosynthetic control and NPQ (in plants and algae) are induced by acidic pH of the thylakoid lumen, an important mechanism to maintain photosynthetic redox balance involves control of the proton motive force *(pmf)* via regulation of the thylakoid ATP synthase (Kanazawa *et al.*, 2017; Takagi *et al.*, 2017). The pH-dependent component of *pmf* (ΔpH), is generated by release of protons to the lumenal side of the thylakoid membrane by water oxidation at PSII and the Q cycle, and proton pumping from the stromal/cytosolic side by cyclic electron transport, as well as consumption of protons on the stromal side. The proton gradient is released mainly via efflux through the ATP synthase, providing the driving force for ATP synthesis. Proton-conductivity of the ATP synthase is therefore an important regulatory factor for adjusting the magnitude of the *pmf*.

In addition to ΔpH, the *pmf* comprises an electric field component ($\Delta\Psi$). $\Delta\Psi$ derives from charge separation within the photosystems and in the Q cycle, the positive charge of protons, and exchange of cations (e.g. K^+, Ca^{2+} and Mg^{2+}) in and anions (e.g. Cl^-) out of the lumen by ion channels and transporters in the thylakoid membrane (Armbruster *et al.*, 2017). ΔpH and $\Delta\psi$ are

thermodynamically equivalent and both drive ATP synthesis (Hangarter & Good, 1982). However, build-up of sufficient ΔpH over the thylakoid membrane is required for induction of photoprotective mechanisms upon sudden increases in light intensity, namely dissipation of excessive excitation energy as heat in NPQ (Niyogi & Truong, 2013; Krishnan-Schmieden *et al.*, 2021) and photosynthetic control (Tikhonov *et al.*, 1981; Degen & Johnson, 2024). These mechanisms prevent over-reduction of the electron transport chain and photodamage to PSI. Conversely, it is also important to down-regulate ΔpH (and consequently, NPQ and photosynthetic control) upon sudden decreases in irradiance in order to maintain sufficient supply of electrons on the acceptor side of the electron transfer chain for carbon fixation in the Calvin–Benson cycle (CBC).

ATP synthase is regulated via several mechanisms. The $F_1\varepsilon$ (epsilon) subunits of the chloroplast (CF_0CF_1) ATP synthase (Feniouk *et al.*, 2006) and the cyanobacterial ATP synthase (Imashimizu *et al.*, 2011; Murakami *et al.*, 2018) have inhibitory roles preventing ATP hydrolysis. $F_1\varepsilon$ undergoes conformational changes triggered by *pmf* generation and changes in ATP/ADP ratio, allowing inhibition of ATP hydrolysis (Richter & McCarty, 1987; Feniouk *et al.*, 2006). Moreover, upon dark-to-light transitions, the chloroplast ATP synthase is activated by thioredoxin (TRX)-mediated reduction of a disulphide in the γ subunit ($CF_1\gamma$) (McKinney *et al.*, 1978; Nalin & McCarty, 1984; Akiyama *et al.*, 2023). $CF_1\gamma$ is kept in an inactive oxidised state in darkness to avoid hydrolysis of ATP by reverse activity or loss of the proton gradient (Hisabori *et al.*, 2013; Kohzuma *et al.*, 2017; Hahn *et al.*, 2018). Interestingly, it was recently reported that the *Chlamydomonas reinhardtii* $CF_1\gamma$, although the conserved disulphide is present, contains a modified hairpin loop in the redox regulatory domain that allows $CrCF_0CF_1$ to remain active also in darkness to facilitate heterotrophic metabolism (Lebok & Buchert, 2024). In plants, maintenance of adequate dark-*pmf* via ATP synthase dark-light regulation is also needed for powering the insertion of new proteins into the thylakoid membrane via the Tat- and Sec-pathways to maintain the integrity of the photosynthetic apparatus (Kohzuma *et al.*, 2017). $CF_1\gamma$ is reduced in seconds upon illumination, which lowers the threshold *pmf* for activation of the ATP synthase (Kramer *et al.*, 1990; Konno *et al.*, 2012; Kohzuma *et al.*, 2017; Nikkanen *et al.*, 2018; Buchert *et al.*, 2021). In turn, ΔpH also facilitates reduction of the $CF_1\gamma$ disulphide bond (Sekiguchi *et al.*, 2024), while dissipation of ΔpH promotes oxidation of $CF_1\gamma$ (Sekiguchi *et al.*, 2022). F- and m-type chloroplast TRX isoforms have been understood to be mainly responsible for light-dependent reduction of $CF_1\gamma$ (Schwarz *et al.*, 1997; Sekiguchi *et al.*, 2020), and chloroplast TRX-like proteins (TrxL2) and 2-cysteine peroxiredoxins (2-CysPrxs) catalyse the oxidation of the subunit in the dark (Yoshida *et al.*, 2018; Sekiguchi *et al.*, 2022). Additionally, *in vivo* studies have revealed the involvement of the NADPH-dependent TRX system (NTRC) in $CF_1\gamma$ reduction in low light conditions (Carrillo *et al.*, 2016; Nikkanen *et al.*, 2016), while the atypical TRX CDSP32 was recently suggested to play a role in reduction of $CF_1\gamma$ in potato (Rey *et al.*, 2024).

Reduction of $CF_1\gamma$ constitutes an on/off switch controlling the activation of the ATP synthase upon the onset of illumination in chloroplasts of plants and algae, and does not occur in mitochondria or in cyanobacteria (Hisabori *et al.*, 2013). The cyanobacterial γ subunit still has a role in preventing ATP hydrolysis however, via an ADP-dependent mechanism (Sunamura *et al.*, 2010). Moreover, the small AtpΘ protein (Song *et al.*, 2022) has been reported to function as an inhibitor of the cyanobacterial ATP synthase in the dark and in low *pmf* conditions, preventing ATP hydrolysis and collapse of the proton gradient. Interestingly, the $F_1\alpha$ (AtpA) and $F_1\beta$ (AtpB) subunits of the ATP synthase also contain conserved Cys residues, and $F_1\alpha$ has been identified as a prospective TRX target in cyanobacteria (Lindahl & Florencio, 2003; Guo *et al.*, 2014), and $F_1\beta$ in plants (Balmer *et al.*, 2006). Moreover, the mitochondrial ATP synthase in *Xenopus laeviis* oocytes is regulated by reversible oxidation of thiols in the $F_1\alpha$ subunit (Cobley *et al.*, 2020).

There are also other regulatory mechanisms that adjust the activation state of the ATP synthase according to the metabolic state of the stroma or cytosol, such as substrate (ADP and P_i) availability; a lack of Pi due to low consumption of ATP by an inactive CBC would lead to a decrease ATP synthase activity, increasing ΔpH and activating photosynthetic control and NPQ to protect PSI from over-reduction (Kanazawa & Kramer, 2002; Avenson *et al.*, 2005; Takagi *et al.*, 2017). High CO_2 supply results in increase of chloroplast ATP synthase activity by a mechanism that is independent of $CF_1\gamma$ redox state (Kiirats *et al.*, 2009; Kohzuma *et al.*, 2013). Another potential regulatory mechanism has been suggested to involve phosphorylation of the $CF_1\beta$ subunit (del Riego *et al.*, 2006), although a more recent study reports that the phosphorylation is unlikely to have a role in controlling ATP synthase activity and is instead involved in CF_1 assembly (Strand *et al.*, 2023).

Additionally, thylakoid conductivity and the *pmf* can be adjusted through the activities of ion channels and transporters in the thylakoid membrane (Spetea *et al.*, 2017). A lack of the K^+/H^+ exchanger KEA3 or the Cl^- channels CLCe and VCCN1 has been shown to affect the *pmf* and/or induction and relaxation of NPQ in plants (Armbruster *et al.*, 2014; Herdean *et al.*, 2016b,a; Wang & Shikanai, 2019; von Bismarck *et al.*, 2023). Similarly, lack of the cyanobacterial K^+ channel SynK resulted in decreased ΔpH generation and impairment of photosynthetic control in the model cyanobacterium *Synechocystis* sp. PCC 6803 (*Synechocystis*) (Checchetto *et al.*, 2012). Controlling the ionic environment of the thylakoid membrane is particularly important to avoid drastic increases in ΔΨ, which result in production of damaging $^1O_2$ via recombination reactions in PSII (Davis *et al.*, 2016).

Plants deficient in the PROTON GRADIENT REGULATION 5 (PGR5) protein suffer from impaired *pmf* generation (Munekage *et al.*, 2002). In plant chloroplasts, PGR5 forms redox-dependent heterodimers with PGRL1 (PGR5-LIKE 1), which have been proposed to mediate or regulate cyclic electron transport (CET) from ferredoxin to the plastoquinone pool (DalCorso *et al.*, 2008; Hertle *et*

al., 2013; Yamamoto & Shikanai, 2019), contributing to *pmf* formation (Wang *et al.*, 2015). More recently, a functional PGRL1-analogue was identified also in cyanobacteria (Dann & Leister, 2019).

The *pgr5* knockout plants are unable to induce photosynthetic control and NPQ during transitions from low to high light (HL) (Munekage *et al.*, 2002; Suorsa *et al.*, 2012; Yamamoto & Shikanai, 2019). Consequently, exposure of *pgr5* mutant plants to HL results in over-reduction of the electron transport chain and photodamage to the iron sulphur clusters of PSI (Tiwari *et al.*, 2016, 2024). Accordingly, the lack of PGR5 is lethal in fluctuating light conditions in *Arabidopsis thaliana (Arabidopsis)* (Tikkanen *et al.*, 2010; Suorsa *et al.*, 2012) and severely inhibits growth of the model C_4 plant *Setaria viridis* (Woodford *et al.*, 2024) as well as of the model green alga *Chlamydomonas reinhardtii (Chlamydomonas)* (Jokel *et al.*, 2018). *Synechocystis* cells deficient in a PGR5-orthologue (SynPgr5) suffer from slightly increased HL-sensitivity (Yeremenko *et al.*, 2005), but no growth impairment was observed in fluctuating light conditions (Allahverdiyeva *et al.*, 2013). Interestingly, however, there is strong selection pressure against overexpression of SynPgr5 (Margulis *et al.*, 2020).

The physiological functions of PGR5 and PGRL1 remain controversial, with some reports linking the proteins to regulation of linear instead of cyclic electron transport from PSI (Nandha *et al.*, 2007; Joliot & Johnson, 2011; Johnson *et al.*, 2014; Tikkanen *et al.*, 2015; Takagi & Miyake, 2018; Rantala *et al.*, 2020; Maekawa *et al.*, 2024), or regulation of the Q-cycle at the cytochrome b_6f complex (Buchert et al., 2020). Impaired *pmf* generation and induction of photoprotection in the *pgr5* mutant could also derive from the inability of the mutant plants to limit the conductivity of the thylakoid membrane under HL (Avenson *et al.*, 2005; Nikkanen *et al.*, 2018; Degen *et al.*, 2023). Interestingly, elevated thylakoid (ATP synthase) conductivity upon HL exposure was not observed in isolated and ruptured *pgr5* mutant chloroplasts (Wang *et al.*, 2018). This suggests that a stromal component that is lost in ruptured chloroplasts plays a role in the effect of PGR5 on thylakoid conductivity.

In the current study, we elucidated the dynamics of *pmf* regulation under light in a variety of photosynthetic organisms focusing on the potential role of PGR5. We performed *in vivo* characterisation of photosynthetic electron transport and *pmf* formation in *Synechocystis*, *Chlamydonomas*, *Arabidopsis*, and *S. viridis.* Our results reveal that in *Arabidopsis*, dynamic regulation of ATP synthase conductivity during fluctuations in light intensity is independent of the thiol redox state of the $CF_1\gamma$ subunit. We show that downregulation of the ATP synthase activity upon transitions to HL depends on PGR5 as well as the thiol redox state of the stroma or cytosol in both chloroplasts and cyanobacteria. Unlike in chloroplasts, PGR5 is not essential for oxidation of the PETC in cyanobacteria. Moreover, we demonstrate that cyanobacterial SynPgr5 is not needed for CET and suggest that the observed effect of plant PGR5 on cyclic electron transport may be an indirect consequence of ATP synthase misregulation and increased photoinhibition of PSI.

MATERIALS AND METHODS

Strains, plant lines and growth conditions

Arabidopsis thaliana WT-gl1 or WT-Col-0, *pgr5-1* (At2g05620 knockout) (Munekage *et al.*, 2002), and *pgr5-Cas* (At2g05620 CRISPR-Cas9 mutant line) (Penzler *et al.*, 2022) plants were grown for 4 weeks under 200 µmol photons in a 12/12h photoperiod before collecting individual leaves for experiments.

For the BiFC experiments, WT *Nicotiana benthamiana* plants were grown under 130 µmol photons m^{-2} s^{-1} at 23°C in a 16/8 hr light/dark photoperiod.

Chlamydomonas reinhardtii WT 137c (progenitor strain of the CC-124 and CC-125 WT strains), *pgr5* knockout and PGR5C complementation strains (Johnson *et al.*, 2014; Jokel *et al.*, 2018) were grown photoautotrophically under continuous 50 µmol photons m^{-2} s^{-1} at 25 °C and 120 rpm in TP medium for four days.

Setaria viridis cv MEO V34-1 *pgr5* knock-out mutant was generated using CRISPR-Cas9 gene-editing as described in detail in (Ermakova *et al.*, 2024). WT plants and plants with *pgr5-3* null alleles described in (Woodford *et al.*, 2024) were analysed. Plants were grown in a controlled environment room with a 16 h : 8 h, light : dark photoperiod, 28°C day and 22°C night, 60% humidity and ambient CO_2 at a light intensity of 300 µmol m^{-2} s^{-1} supplied by 1000 W red sunrise 3200K lamps (Sunmaster Growlamps, Solon, OH, USA). Youngest fully expanded leaves of 3–4-week-old plants were used in analysis.

WT, Δ*pgr5*, Δ*flv3* (Helman *et al.*, 2003) and Δ*pgr5 flv3 Synechocystis* sp. PCC 6803 strains as well as WT *Synechococcus elongatus* sp. PCC 7942 cells were grown under continuous 50 µmol photons m^{-2} s^{-1} at 30 °C and air-level [CO_2] in pH 7.5 BG-11 medium. Unless stated otherwise, cultures were grown for 4 days in 30 ml flasks, then pelleted and resuspended in fresh BG-11 at an appropriate chlorophyll concentration for each experiment. For the growth curves under fluctuating light, WT, *Δpgr5* and *Δpgr5 flv3* cells were grown for 7 days in conditions where light intensity was held at 20 µmol photons $m^{-2}s^{-1}$ and increased to 500 µmol photons $m^{-2}s^{-1}$ for 30 sec every 5 min. Samples were taken and $OD_{750\ nm}$ measured with a spectrophotometer every 24h. For the experiment in Figure 5, cells were grown in a regime in which light intensity fluctuated between 1 min periods of 25 and 500 µmol photons $m^{-2}s^{-1}$.

Construction of Δ*pgr5* and Δ*pgr5 flv3* knockout mutants

The upstream and downstream flanking sequences of the *pgr5* (*ssr2016*) gene and the *aphI* (Km^R) gene replacing the *ssr2016* open reading frame were amplified from genomic DNA of Δ*pgr5* mutant generated earlier in a different *Synechocystis* WT background as described in (Allahverdiyeva *et al.*, 2013). After transformation into *Synechocystis* sp. PCC 6803 WT strain and the Δ*flv3* strain (Helman *et al.*, 2003), the transformants were selected on BG-11 plates with 50 µg/ml kanamycin. Complete segregation of the mutation was confirmed by PCR with specific forward primer 5′-AGCCAAACCGCATCTAACG-3′ and reverse primer 5′-TTCATAACGCCTCCGGTC-3′. The expected PCR fragment length was 0.7 kb for the WT and 1.7 kb for the mutant (Supplementary Fig. S1). The mutation in the *flv3* open reading frame was confirmed by using forward primer 5′-GTACGGCATGTTCACTACC-3′ and reverse primer 5′- GATCAGCGTTAGCCTGTAA-3′, and the expected PCR fragment length was 1.0 kb for the WT and 2.6 kb for the mutant (Supplementary Fig. S1). Two separate clones of Δ*pgr5* were used interchangeably for the experiments, as no difference was detected in their phenotypes.

Electrochromic shift (ECS) measurements

Individual *Arabidopsis* leaves were measured with the Dual-PAM 100 spectrophotometer (Walz) and its P515/535 accessory module (Schreiber & Klughammer, 2008) as described earlier (Nikkanen *et al.*, 2018; Guinea Diaz *et al.*, 2020). For the experiment in Figure 1, dark-adapted (30 min) leaves were exposed to a light regime fluctuating between 1 min periods of 50 and 825 µmol photons m^{-2} s^{-1}, with 250 ms dark intervals administered every 5 seconds for the first 30 seconds and every 10 seconds thereafter. For the methyl viologen (MV) experiment, detached leaves were dark-incubated overnight on water with 0.05% Tween-20 ± 1 µM MV. In the ECS measurement, dark intervals of 450 ms were administered every 4 s until 28 s during 95 µmol photons $m^{-2}s^{-1}$ of actinic illumination, every 10 s between 28 and 58 s, every 30 s between 58 and 298 s, every 4 s after transition to 825 µmol photons $m^{-2}s^{-1}$ between 298 and 318 s, and every 30 s thereafter. 2,000 Hz pulse frequency of the measuring light was used. ΔECS_T values were normalised to the ΔECS measured upon a 20 µs single-turnover saturating flash administered with the Dual-PAM 100 on dark-adapted leaves (ΔECS_{ST}) (Mathiot & Alric, 2021). For the NEM experiment, detached leaves were incubated in dark on water with 0.05% Tween-20 ±0.1 mM NEM for 2 hours before the experiment. *Chlamydomonas* cultures and *S. viridis* leaves were measured using the same protocol as *Arabidopsis*, with *Chlamydomonas* chlorophyll concentration set to 20 Chl µg ml^{-1}.

ECS changes were measured from *Synechocystis* and *Synechococcus* cells by monitoring the 500-480 nm absorbance difference signal (Viola *et al.*, 2019) using a JTS-10 spectrophotometer (BioLogic) as described in (Nikkanen *et al.*, 2020). Cells were pelleted and resuspended in fresh BG-11 at 7.5 µg Chl ml^{-1}. When appropriate, 0.1 mM NEM was added to the samples before a 5 min dark-adaption prior to the measurement. Each measurement was also conducted with the cells illuminated only by the measuring light flashes, and the ECS changes recorded were then subtracted from the measurements under green actinic light, in order to control for any actinic effects of the measuring light. A moderate (60 µmol photons m^{-2} s^{-1}, relative to growth light of 50 µmol photons m^{-2} s^{-1}) rather than a low actinic light intensity was used in fluctuating light to allow a sufficient signal-to-noise ratio for dark-interval relaxation kinetics (DIRK) analysis. The cyanobacterial ECS signals were not normalised to ECS_{ST} due to a low signal-to-noise ratio of single turnover traces. Instead, a constant chlorophyll concentration was used.

The *pmf* and g_H+ parameters were determined as the difference between magnitude of the ECS signal in light – y0 value of a first-order fit to the decay kinetics of the signal during a dark interval, and the inverse of the time constant of the fit, respectively, while v_H+ was derived as *pmf* x g_H+ (Cruz *et al.*, 2005). Fitting and data processing was done with the OriginPro 2024b (OriginLab) software.

Saturating pulse analysis of chlorophyll fluorescence and $P700^+$

The extents of the donor side and acceptor side limitations of PSI, Y(ND) and Y(NA), respectively, were determined under fluctuating light conditions by a saturating pulse analysis of the $P700^+$ signal using the Dual-PAM 100 (Klughammer & Schreiber, 2008). Chlorophyll autofluorescence was simultaneously recorded to determine the Y(NPQ) parameter (in *Arabidopsis*) as described by (Schreiber *et al.*, 2008). Saturating pulses (8000 µmol photons m^{-2} s^{-1} for *Arabidopsis* and 3000 µmol photons m^{-2} s^{-1} for *Synechocystis*) were administered every 15 seconds during illumination.

Deconvoluted P700, plastocyanin, and ferredoxin redox changes

The deconvoluted plastocyanin (PC), P700, and ferredoxin redox changes were determined by NIR absorbance difference spectroscopy using the DUAL-KLAS-NIR spectrophotometer (Walz) (Klughammer & Schreiber, 2016). CET and LET at PSI in *Synechocystis* were quantified using DIRK analysis according to (Theune *et al.*, 2021) with modifications. *Synechocystis* cells were pelleted and adjusted to 15 µg Chl ml^{-1} with fresh BG-11. Cells were pre-illuminated for 2 min with 500 µmol photons m^{-2} s^{-1}, followed by administration of 100 dark intervals of 20 ms. The 100 decay traces

were averaged and initial slopes of the PC and P700 decay curves were used to calculate J_{PSI}. J_{PSI}-CET was determined by repeating the same experiment in the presence of 10µM DCMU to block electron transport from PSII. The NIRMAX script (Klughammer & Schreiber, 2016) modified for cyanobacteria was used to determine the maximal oxidation of PC and P700 and maximal reduction of ferredoxin (Fed). The model spectra for the deconvolution of PC, P700, and Fed redox changes in *Synechocystis* were measured as described in (Nikkanen *et al.*, 2020). Arabidopsis NIRMAX measurements of dark-adapted leaves were conducted as described in (Nikkanen *et al.*, 2019). Reduction kinetics of Fed under far red light were measured after running the NIRMAX script, illuminating detached leaves for 1 second with intensity 20 far-red light.

Cytochrome *f* redox changes

Detached leaves from 4-weeks-old WT-gl1 and *pgr5-1* Arabidopsis were dark-adapted for 5 min, after which the cytochrome *f* redox kinetics were measured as time-resolved absorbance changes at 554 nm with a baseline drawn between 546 and 573 nm during and after five seconds of illumination with 500 µmol photons m^{-2} s^{-1} of green light, using the JTS-10 spectrophotometer and sequential measurements with appropriate interference filters (10 nm FWHM, Edmund Optics). Scattering artifacts were minimised by BG39 filters (Schott). The cytochrome *f* post-illumination re-reduction rates ($k_{f\ red}$ s^{-1}) were obtained by fitting the post-illumination kinetics over 300 ms to a first-order exponential function.

Protein thiol alkylation and SDS-PAGE

4-week-old *Arabidopsis* WT-Col-0 and *pgr5*-Cas plants were dark-adapted, exposed to a light regime fluctuating between 1-minute periods of 50 and 800 µmol photons m^{-2} s^{-1}. Samples (individual leaves) were taken every 20 seconds and quickly placed in 10 % TCA solution to freeze the thiol redox state of proteins. TCA precipitation, alkylation of thiols with MALPEG-5000, and SDS-PAGE was then performed as described in Nikkanen et al., (2016). Briefly, free thiol groups were first alkylated with NEM. Following alkylation, disulphide bonds in proteins were reduced with dithiothreitol (DTT), and the resulting thiols were then alkylated using methoxypolyethylene glycol maleimide Mn 5000 (MAL-PEG, Sigma-Aldrich). This treatment makes the in-vivo oxidised forms of proteins migrate more slowly than reduced ones in SDS-PAGE. MV-treated WT-Col-0 leaves (see above) were illuminated in growth conditions for 0, 30, 90, or 180 min before sample collection and placement in 10% TCA.

Total protein extractions from *Synechocystis* cells were done as described in (Zhang *et al.*, 2009) and from *N. benthamiana* leaves by grinding the tissue in a buffer with 100 mM Tris-HCl pH 8, 50 mM

EDTA, 250 mM NaCl, and 0.75% SDS, heating for 10 min at 68°C, and centrifuging for 10 min at 14,000 rpm. Protein concentration was determined by the DC Protein Assay Kit (Bio-Rad, based on the Lowry assay). Sodium dodecyl sulphate polyacrylamide gel electrophoresis (SDS-PAGE) and immunoblotting were performed as previously described (Nikkanen *et al.*, 2016). 4–15% Mini-PROTEAN TGX precast gels (Bio-Rad) were used for electrophoresis except for Figure 5, for which 12% polyacrylamide gels with 6M urea were cast. PVDF membranes were probed with antibodies raised against $CF_1\gamma$ (Agrisera, AS08 312), FBPase (courtesy of Dr M. Sahrawy), AtpB (Agrisera, AS), Flv3 (Genscript), NTRC (Lepistö *et al.*, 2009), or 2-CysPrx (courtesy of Prof. F.□J. Cejudo).

Membrane Inlet Mass Spectrometry (MIMS)

Synechocystis in vivo O_2 and CO_2 gas fluxes were monitored in real-time by membrane inlet mass spectrometry (MIMS) as described earlier (Mustila *et al.*, 2016), with O_2 uptake distinguished from O_2 evolution by enrichment of the $^{18}O_2$ isotope in the medium. Chlorophyll concentration was set to 10 µg Chl ml^{-1}, 1.5 mM $NaHCO_3$ was added, and cells were dark-adapted for 15 min prior to the measurements. Gas exchange was monitored under 500 µmol photons $m^{-2}s^{-1}$ illumination for 5 min. See legend for Fig. 2i for experimental details.

Bimolecular Fluorescence Complementation (BiFC) tests

In planta protein–protein interaction tests by bimolecular fluorescence complementation (BiFC) were conducted as described earlier (Nikkanen *et al.*, 2016, 2018). *Nicotiana benthamiana* plants were used for transient expression of fusion constructs via *Agrobacterium tumefaciens* strain GV3101 infiltration. Imaging was done 3 days after infiltration using a Zeiss LSM780 confocal microscope. Construction of the AtPGR5:YFP-C and AtNdhS:YFP-N expression vectors for YFP-fusion proteins is described in (Nikkanen *et al.*, 2018) and construction of the $AtCF_1\gamma$:YFP-N and AtTRXx:YFP-C vectors in (Nikkanen *et al.*, 2016).

***In silico* modelling**

The ClusPro 2.0 protein-protein docking service (Kozakov *et al.*, 2017) was used to perform molecular docking of the AtPGR5 (Uniprot identifier Q9SL05) / SoCF1γ (P05435) / SoCF1□ (P00833) interaction complex, as well as the AtPGR5 / AtPGRL1a (Q8H112)/ AtTRXm4 (Q9SEU6) complex. The predicted chloroplast transit peptides (amino acid residues 1–60, 1–60, and 1–82) for AtPGR5, AtPGRL1a, and AtTRXm4, respectively) were removed from the structures before docking.

The amino acid sequences for *Synechocystis* genes *sll1327*, *slr1330* and *ssr2016* were retrieved from the Uniprot database (entries P17253, P26533, and P73358, respectively). AlphaFold2 Multimer Google Colab notebook (Mirdita *et al.*, 2022) was used to model the interaction complex using 6 recycles and pdb100 template mode, with Amber relaxation of the best model. The model with the best pTM score was selected for visualisation using the Mol* 3D viewer (Sehnal *et al.*, 2021). The *Spinacia oleracea* chloroplast ATP synthase structure (Hahn *et al.*, 2018) was retrieved from the RCSB PDB database (entry 6FKF), while overlaying with the SoCF1γ/AtPGR5 interaction model as well as modelling of electrostatic surface charges was performed with ChimeraX (Meng *et al.*, 2023).

Statistical tests

ANOVA, Tukey's tests for significance, Student's T-tests, and linear mixed effects modelling (LMEM) were performed using the OriginPro 2024 software and its LMEM App. The LMEM models included gH□ as the dependent variable, *pmf* as a continuous covariate, genotype and light intensity as fixed factors, and biological replicate as a random factor. Significance was assessed using the F-tests provided by the software.

RESULTS

Dynamic changes in thylakoid conductivity are independent of the thiol redox state of $CF_1\gamma$ in plants

In plants and algae, measurement of dark-interval relaxation kinetics (DIRK) of the electrochromic shift (ECS) signal has been widely used for *in vivo* determination of the magnitude of the *pmf*, partitioning of the *pmf* between ΔpH and ΔΨ, as well as the conductivity of the thylakoid membrane, which is mainly determined by the activity of ATP synthase (Sacksteder & Kramer, 2000; Cruz *et al.*, 2001, 2005; Schreiber & Klughammer, 2008; Bailleul *et al.*, 2010). Recently, a reliable method to measure ECS has also been developed for cyanobacteria (Viola *et al.*, 2019; Nikkanen *et al.*, 2020; Santana-Sánchez *et al.*, 2023).

Time-resolved ECS analysis in wild type (WT) *Arabidopsis* revealed that upon the onset of illumination of dark-adapted leaves, the conductivity of the ATP synthase (g_H+) initially decreased for c.a. 30 s (Fig. 1a), as observed previously (Nikkanen *et al.*, 2018; Guinea Diaz *et al.*, 2020). This initial decrease in g_H+ allowed transient build-up of *pmf* (Fig. 1b) and induction of NPQ and photosynthetic control (as indicated by donor-side limitation of PSI) (Fig. 1d–e) in order to avoid over-reduction of the electron transport chain when redox-regulated CBC enzymes are not yet activated (i.e. reduced).

After the initial decrease, at c.a. 30 s of illumination, g_H+ started to increase gradually, resulting in decrease of *pmf* (Fig. 1a–d). Importantly, these changes in g_H+ did not correlate with the thiol redox state of $CF_1\gamma$. $CF_1\gamma$ was rapidly reduced at the onset of illumination, becoming almost fully reduced after 20 s, and remained reduced thereafter (Fig. 1f). In contrast, the CBC enzyme Fructose-1,6-bisphosphatase (FBPase) remained mostly oxidised (inactive) for a full minute in low light, and only became partially reduced when leaves were exposed to HL (Supplementary Fig. S2).

In a light regime where light intensity alternates between periods of low light (LL) and HL, mimicking natural fluctuations, intricate regulatory dynamics of the *pmf* and g_H+ could be observed. During LL phases, g_H+ increased substantially, which contributed to a rapid decline in *pmf* (Fig. 1a–b). This upregulation of g_H+ allowed relaxation of photosynthetic control (as inferred from donor-side limitation of PSI) and NPQ (Fig. 1e–f), allowing sufficient supply of electrons to stromal reactions. Similarly to downregulation of g_H+ during dark-to-light transitions, the upregulation of g_H+ during LL happened independently of the thiol redox state of $CF_1\gamma$, which remained fully reduced throughout the change in light intensity (Fig. 1e).

In contrast to LL phases, g_H+ was rapidly downregulated in WT leaves during HL phases (Fig. 1a), enabling sufficient *pmf* build-up (Fig. 1b) for induction of photosynthetic control and NPQ (Fig. 1d–e). Again, the decrease in g_H+ did not coincide with oxidation of $CF_1\gamma$, which remained fully reduced (Fig. 1f).

These results demonstrate that ATP synthase activity undergoes dynamic regulation under fluctuating light in Arabidopsis, and that this regulation is independent of $CF_1\gamma$ redox state and must occur via another mechanism.

Thylakoid conductivity is dynamically regulated under fluctuating light also in cyanobacteria and unicellular algae

When WT *Synechocystis* cells were subjected to sudden fluctuations between moderate light (ML) and HL, time-resolved ECS-DIRK measurements revealed downregulation of g_H+ during HL phases (Fig. 2a), resembling that observed in *Arabidopsis.* As in plants, this downregulation likely occurs to maintain an adequate *pmf* (Fig. 2b) for induction of photosynthetic control. Accordingly, strong donor side limitation of PSI (Y(ND)) was measured during HL phases (Fig. 2e) indicative of limitation of electron transport from Cyt b_6f. In contrast to *Arabidopsis*, g_H+ remained low during the ML phases of the experiment (Fig. 2a).

We also probed the *pmf* and g_H+ dynamics under fluctuating light in the unicellular green alga *Chlamydomonas.* While *pmf* underwent similar changes as in plants and in cyanobacteria (Fig. 3b), no

clear downregulation of g_H+ was observed during HL, and during the LL phases g_H+ remained low (Fig. 3a).

PGR5 is needed for downregulation of thylakoid conductivity under strong illumination across photosynthetic organisms

During dark-to-LL transitions, the *Arabidopsis pgr5* mutant plants had a lower *pmf* than WT (Fig. 1B), as shown previously and attributed to lower linear electron transport rates (Nikkanen *et al.*, 2018). In fluctuating light, the *pgr5* mutants maintained a significantly higher gH+ than WT during HL phases (Fig. 1a), resulting in partial loss of *pmf* (Fig. 1b), in agreement with previous studies (Avenson *et al.*, 2005; Nikkanen *et al.*, 2018). The mutant plants also exhibited impaired induction of NPQ (Fig. 1d) and photosynthetic control, resulting in an inability to oxidise P700 (Y(ND), Fig. 1e) and low PSI quantum yield (Supplementary Fig. S3a) due to high acceptor side limitation (Supplementary Fig. S3b). Interestingly, and in contrast to their behaviour during HL phases, *pgr5* mutant plants showed a lower g_H+ and slightly lower *pmf* than WT during LL phases (Fig. 1a–b), which was due to diminished proton flux (vH+) (Fig. 1c). A small amount of reduced $CF_1\gamma$ was detected in the dark in *pgr5*, but under the fluctuating light treatment the redox state of $CF_1\gamma$ was indistinguishable from WT, as $CF_1\gamma$ was rapidly reduced upon illumination and maintained as such throughout the fluctuating light treatment also in *pgr5* (Fig. 1g).

As it has been proposed that PGR5 deficiency results in impaired Q cycle activity in *Chlamydomonas* (Buchert *et al.*, 2020), we confirmed that the elevated gH+ values in Arabidopsis *pgr5* are not caused by diminished charge separation in the Q cycle during the dark intervals. No difference in post-illumination re-reduction rates of cytochrome *f* was detected between WT and *pgr5* (Supplementary Fig. S4), indicating that the elevated gH+ in *pgr5* does indeed derive from increased proton conductivity of the thylakoid membrane.

Next, we sought to elucidate the bottleneck in the electron transport chain that impairs PSI oxidation in *pgr5*. It was proposed recently that Fed binding to PSI is impaired due to damage of F_A and F_B iron-sulphur clusters in *pgr5* already under moderate light (Tiwari *et al.*, 2024). Since it has also been suggested that the rate of Fed oxidation is primarily determined by the linear electron transport rate (Takagi & Miyake, 2018), we compared the Fed reduction and oxidation kinetics between WT and *pgr5* during and after a 1 s pulse of far-red light to minimise the contribution of linear electron flow and examine just the ability of PSI to reduce, and acceptors to oxidise Fed. Our results show that both reduction and re-oxidation kinetics of Fed are slowed down in *pgr5*, while oxidation of PC was increased and oxidation of P700 remained similar to WT (Supplementary Fig. S5), in agreement with the proposal by Tiwari et al. (2024).

The *Arabidopsis pgr5-1* mutant used in our experiments has been reported to also contain an additional mutation in the At2g1724 gene, which slightly exacerbates PSI photoinhibition in the mutant (Wada *et al.*, 2021). Mutants where an intact At2g1724 has been re-introduced (*pgr5*^{hope1} and *pgr5-Cas*) are, however, also unable to induce photosynthetic control to oxidise PSI (Wada *et al.*, 2021), and have similarly elevated g_H+ and diminished *pmf* as the *pgr5-1* mutant (Penzler *et al.*, 2022; Maekawa *et al.*, 2024). While it is therefore unlikely that the At2g1724 mutation in *pgr5-1* plants would have a significant effect on the phenotypes examined in the current study, we confirmed this by repeating the ECS experiment (Fig. 1a–c) also with the *pgr5-Cas* mutant (Penzler *et al.*, 2022). Results with *pgr5-Cas* plants were similar to the ones with *pgr5-1*, apart from the decrease in *pmf* during initial dark-to-LL transitions being less prominent in *pgr5-Cas* plants than in *pgr5-1* in comparison to WT (Supplementary Fig. S6). Moreover, while a diminished proton flux (v_H+) in LL and immediately upon shifts to HL was measured in *pgr5-1* mutants in comparison to WT (Fig. 1c), this decrease was absent in *pgr5-Cas* plants, which instead exhibited elevated v_H+ during the first HL phase (Supplementary Fig. S6c). In order to examine if this elevation of vH+ or changes to gH+ were linked to altered mitochondrial respiration, we repeated the ECS experiment in the presence of potassium cyanide (KCN) and salicylhydroxamic acid (SHAM), inhibitors of Complex IV and alternative oxidase (AOX) in mitochondrial respiration, respectively. Compared to WT, *pgr5*-Cas plants maintained elevated gH+ also in these conditions, while vH+ and *pmf* are lower than WT in LL but higher than WT in HL (Supplementary Fig. S7). These results indicate that the elevated gH+ and vH+ observed in HL in *pgr5* mutants do not derive from increased mitochondrial respiration.

We proceeded to investigate whether lack of SynPgr5 affects regulation of g_H+ in *Synechocystis*. Elevated g_H+ was indeed detected upon exposure of Δ*pgr5* cells to HL after illumination in moderate light (ML) in a fluctuating light regime (Fig. 2a, d), concomitant with lowered (albeit statistically insignificantly) *pmf* towards the end of the second HL cycle (Fig. 2b). The increased g_H+ was not due to an elevated amount of ATP synthase, as the protein level of AtpB remained unchanged in the mutant (Supplementary Fig. S8). Despite the elevated g_H+ and in contrast to AtPGR5-deficient *Arabidopsis*, no decrease in PSI quantum yield (Supplementary Fig. S3c), donor-side limitation (indicative of impairment of photosynthetic control) (Fig. 2e) or increase in acceptor side limitation of PSI (Fig. 2f) was detected during transitions to HL in *Synechocystis* Δ*pgr5* cells. Interestingly, a slight, albeit statistically non-significant decrease in donor side limitation of PSI was detected in Δ*pgr5* upon transitions from HL to LL (Fig. 2e).

The ability of the *Synechocystis* Δ*pgr5* strain to maintain sufficient PSI oxidation for unimpaired photosynthetic activity may be due to the strong electron sink capacity of the Mehler-like reaction catalysed by flavodiiron proteins (FDPs) under light (Allahverdiyeva *et al.*, 2013). Therefore, we tested the PSI oxidation capacity of a Δ*flv3 pgr5* double mutant strain, which is deficient in both

SynPgr5 as well as the Flv1/3 hetero-oligomers (Supplementary Fig. S1) which are mainly responsible for the strong, rapidly induced Mehler-like reaction (Santana-Sanchez *et al.*, 2019). We detected slightly but non-significantly aggravated acceptor side limitation of in the double mutant in comparison to the Δ*flv3* single mutant during initial LL-to-HL transitions (Fig. 2f). The additional effect of Pgr5 deficiency was minor compared to lack of Flv3, and no additional aggravation of ferredoxin redox kinetics, CO_2 fixation, or O_2 evolution was observed in Δ*flv3 pgr5* in comparison to Δ*flv3* (Supplementary Fig. S9). These results indicate that SynPgr5 may affect PSI oxidation also in cyanobacteria, but its importance is minor compared to plants, while flavodiiron proteins have a crucial role. This was also reflected in the growth phenotypes of the strains. In agreement with previous results (Allahverdiyeva *et al.*, 2013), no impairment of growth was detected between WT and Δ*pgr5* under fluctuating light (1 min LL / 1 min HL), with Δ*pgr5* even growing slightly faster than WT, while additional deficiency of Flv3 in Δ*pgr5 flv3* and Δ*flv3* resulted in severe impairment of growth (Fig. 2g).

The Δ*flv3* mutant showed a decreased g_H+ in the HL phases of fluctuating light (Fig. 2a), which allowed it to compensate for diminished v_H+ (Fig. 2c) and maintain WT-level *pmf* (Fig. 2b). The Δ*pgr5 flv3* double mutant, however, exhibited WT-like g_H+, v_H+, and *pmf* (Fig. 2a–c), indicating that the downregulation of g_H+ observed in Δ*flv3* is also at least partly dependent on SynPgr5.

To clarify whether SynPgr5 is involved in CET in *Synechocystis* as previously concluded (Yeremenko *et al.*, 2005; Dann & Leister, 2019), we quantified the rates of CET and linear electron transport (LET) in WT and Δ*pgr5* cells using DIRK analysis of near-infrared absorbance difference signals, as described by (Theune *et al.*, 2021). Our results showed that the CET rate was not decreased in the deletion mutant (Fig. 2h), indicating that SynPgr5 is not involved in CET, at least in steady state conditions. It has been previously reported that a *Synechocystis* Δ*pgr5* mutant has an accelerated rate of P700 oxidation under far-red light as measured with the Dual-PAM 100 spectrophotometer (Dann & Leister, 2019), which can be an indication of decreased CET, although results from such assays should be interpreted with caution (Fan *et al.*, 2007). In contrast to the previous report, we detected no difference between WT and Δ*pgr5* in far-red-induced P700 oxidation rate when measured as the deconvoluted P700 signal using the Dual-KLAS-NIR instrument (Supplementary Fig. S10). There results suggest that SynPgr5 is not involved in CET.

Near-infrared spectroscopy revealed no significant differences in the deconvoluted redox signals for ferredoxin (Fed), plastocyanin (PC) or P700 between WT and Δ*pgr5* cells upon onset of strong illumination (Supplementary Fig. S11a). Moreover, analysis of *in vivo* O_2 and CO_2 gas exchange by membrane inlet mass spectrometry (MIMS) showed that oxygen evolution (Supplementary Fig. S11b), dark respiration rate (Supplementary Fig. S11c), light-induced O_2 uptake rate indicative of FDP activity (Supplementary Fig. S11b, d), as well as CO_2 fixation (Supplementary Fig. S11e) were

all unchanged in Δ*pgr5* in comparison to WT cells. When cells were grown under fluctuating light and O_2 gas exchange was measured under similar conditions, however, a slightly elevated light-induced O_2 uptake rate was observed in Δ*pgr5*, although the difference was statistically significant only during the first HL phase (Fig. 2i).

There is no PGR5 orthologue identified in the genome of another cyanobacterial model species, *Synechococcus elongatus* PCC 7942 (*Synechococcus*) (Shimakawa *et al.*, 2016). We therefore proceeded to investigate whether the regulation of g_H+ in response to fluctuating light conditions in *Synechococcus* differs from *Synechocystis.* Interestingly, no major difference was observed in comparison to the g_H+ kinetics in *Synechocystis*, with down-regulation of g_H+ occurring during the HL phases after an initial increase (Supplementary Fig. S12). This suggests that the downregulation of g_H+ in HL is achieved via a different mechanism in *Synechococcus*.

Elevated g_H+ under HL was also observed in the *Chlamydomonas pgr5* mutant, in comparison to WT or a CrPGR5 complementation strain (Fig. 3a). Interestingly, this did not result in lower *pmf* under HL due to elevated proton flux (v_H+) (Fig. 3b, c). We confirmed that the potential presence of damaged PSI centres in *pgr5* (Tiwari et al., 2024) did not result in major overestimation of the *pmf* and vH+ parameters by also plotting the *Chlamydomonas* ECS data normalised only by Chl concentration (Supplementary Fig. S13). Finally, the increase in g_H+ during the HL phases of a fluctuating light regime was also detected in a *pgr5* mutant of the model C_4 grass *S. viridis* (Supplementary Fig. S12). Similarly to Arabidopsis but unlike *Synechocystis*, both *Chlamydomonas* (Jokel *et al.*, 2018) and *S. viridis* (Woodford *et al.*, 2024) *pgr5* mutants suffer from an inability to oxidise PSI in HL.

It has been suggested that the elevated gH+ in *pgr5* mutants is simply a consequence of lower *pmf*, and that when *pmf* is the same, there would be no difference in gH+ between WT and *pgr5* (Kappel *et al.*, 2023). However, this correlation was made based on steady state measurements. When we plotted the gH+ values from our time-resolved ECS measurements in fluctuating light as a function of *pmf*, the correlation between the two parameters differed dramatically between WT and *pgr5* mutants in all species examined in the current study (Fig. 4). Linear mixed effects models (Supplementary Tables S1–S7) revealed that Arabidopsis *pgr5-1* mutants exhibited a significantly elevated gH□ in HL compared to WT independently of *pmf* (p=0.001), with an estimated difference of +5.6 gH+ units across all *pmf* values. Notably, *pmf* was not a significant predictor of gH□ in this condition (p=0.74). Similarly, gH+ values increased independently of *pmf* in HL also in Arabidopsis *pgr5*-Cas (+6.89, p=0.001), and in the full dataset in *Synechocystis* Δ*pgr5* (+12.3, p=0.0154), *Chlamydomonas pgr5* (+5.72, p=0.003, and *S. Viridis pgr5* (+10.7, p=0.010). These results indicate that the effect of PGR5 on gH+ is not an indirect consequence of diminished *pmf* in any of the studied organisms, and highlight a conserved function of PGR5 in regulation of the proton conductivity of ATP synthase from cyanobacteria to chloroplasts in algae, C_3, and C_4 plants.

Elucidating the mechanism of redox-dependent inhibition of thylakoid conductivity

We have previously shown that increasing the reducing capacity of the chloroplast thiol redox regulation systems through overexpression of NTRC in *Arabidopsis* intensifies the downregulation of g_H+ upon increases in light intensity (Nikkanen *et al.*, 2018). We therefore proceeded to investigate potential thiol regulation of thylakoid conductivity or ATP synthase activity, as well as the role of PGR5 in it.

Addition of methyl viologen (MV) results in lowered conductivity of the thylakoid membrane, which has been interpreted as prevention of TRX-mediated reduction of the $CF_1\gamma$ disulphide (Kramer & Crofts, 1989). MV facilitates electron transfer from PSI or reduced ferredoxin to O_2 (the Mehler reaction), resulting in generation of ROS (Fujii *et al.*, 1990; Sétif, 2015; Shapiguzov *et al.*, 2019, 2020). However, MV is also able to donate electrons to redox-regulated enzymes such as nitrite reductase in spinach (Hirasawa & Tamura, 1980) and glutathione reductase in yeast (Llobell *et al.*, 1986). To further elucidate the relationship between stromal/cytosolic thiol redox state and PGR5-dependent downregulation of thylakoid conductivity, we investigated the effects of MV on chloroplastic thiol-regulated enzymes and *pmf* in *Arabidopsis.* We first determined the *in vivo* thiol redox states of the chloroplast redox enzymes as well as $AtCF_1\gamma$ in presence or absence of 1 µM MV. Although electron supply to the TRX systems from PSI is limited by MV, addition of MV caused strong reduction of the 2-cysteine peroxiredoxin (2-CysPrx), FBPase, and $CF_1\gamma$ pools even in darkness (Fig. 5a). NTRC, whose redox state is mostly unaffected by light conditions, thereby acting as a buffer system for plastidial redox state (Nikkanen *et al.*, 2018; Zimmer *et al.*, 2021), also became strongly reduced after 90 min of illumination when treated with MV (Fig. 5a).

Next, we investigated the effect of MV on regulation of *pmf* and g_H+ in WT *Arabidopsis* leaves. Upon illumination of dark-adapted leaves, g_H+ was initially significantly higher in MV-treated WT leaves than in control leaves (Fig. 5b), most likely due to dark-reduction of $AtCF_1\gamma$ by MV (Fig. 5a). As illumination continued, g_H+ diminished in MV-treated leaves and remained at a very low level throughout the rest of the experiment (Fig. 5c). This results in very high *pmf* (Fig. 5d) and NPQ (Shapiguzov *et al.*, 2020). In contrast, MV-treatment of *pgr5* mutant leaves caused only a minor decrease in g_H+ and increase in *pmf* during illumination, and in HL g_H+ was in fact higher in MV-treated *pgr5* mutant than in WT control leaves (Fig. 5c–d), suggesting that the MV-mediated g_H+ decrease is dependent on AtPGR5.

We also investigated the effect of perturbing the thiol redox state of the cell on thylakoid conductivity in *Synechocystis.* As moderate concentrations of MV have only minor effects on cyanobacterial

electron transport (Sétif, 2015), with no significant impact on g_H+ observed after addition of 0.5 mM MV (Supplementary Fig. S15), we opted to test the effect of supplementation with the thiol-alkylating agent N-ethylmaleimide (NEM). Addition of 0.1 mM NEM to WT *Synechocystis* cultures resulted in a significant increase in g_H+ after 5 seconds of illumination (Fig. 6a), similarly to results recently reported for another maleimide compound 2-methylmaleimide (Hubáček *et al.*, 2024). In Δ*pgr5* cells, only a slight, statistically non-significant NEM-induced increase in g_H+ was observed. In *Synechococcus*, which does not have PGR5, NEM did not have a significant effect on g_H+ (Fig. 6b). Finally, we also tested the effect of NEM on g_H+ in *Arabidopsis* WT and *pgr5* mutant leaves, repeating the fluctuating light experiment from Figure 1. NEM decreased g_H+ throughout the experiment in WT (Fig. 6c), albeit not as dramatically as MV treatment. In contrast, *pgr5* mutant leaves did not respond to NEM treatment during the first LL-HL cycle (Fig. 6c). During subsequent cycles g_H+ in NEM-treated *pgr5* mutant leaves decreased slightly in comparison to untreated *pgr5* mutant leaves, while still remaining significantly higher than untreated WT leaves (Supplementary Fig. S16) in HL.

These results provided evidence that PGR5 is involved in a redox-dependent regulatory mechanism of ATP synthase activity that is distinct from $F_1\gamma$ redox state. Interestingly, it has been reported that PGR5 from cucumber (*Cucumis sativus L.*) can interact with the AtpB subunit of the chloroplast ATP synthase in yeast-two-hybrid tests (Wu *et al.*, 2021)**.** To investigate the ability of PGR5 to directly interact with ATP synthase *in planta*, we performed bimolecular fluorescence complementation (BiFC) tests between AtPGR5 and At$CF_1\gamma$. Indeed, strong YFP fluorescence co-localising with chlorophyll autofluorescence was detected, indicating interaction between the two proteins in chloroplast thylakoid membranes (Fig. 7a). As negative controls we performed BiFC tests between AtPGR5 and the NdhS subunit of the chloroplast NAD(P)H dehydrogenase-like complex, another major thylakoid protein complex, as well as At$CF_1\gamma$ and Thioredoxin x, a chloroplast protein similar in size to AtPGR5 (Supplementary Fig. S17). AtCF1γ +AtTRXf1 and AtPGRL1+AtPGR5 interactions were used as positive controls (Supplementary Fig. S18a–b), as both interactions are well established in previous studies (Nikkanen *et al.*, 2016, 2018). No cleaved YFP fragments were detected in immunoblots with an antibody against YFP using in total protein extracts from *N. benthamiana* leaves transiently expressing the At$CF_1\gamma$:YFP-N fusion protein (Supplementary Fig. S18c).

We also performed molecular docking of *Spinacia oleracea* $CF_1\gamma$ and CF_1□ (Hahn *et al.*, 2018) with an available AtPGR5 structural model using the ClusPro 2.0 protein-protein docking service (Kozakov *et al.*, 2017). As the $CF_1\varepsilon$-subunit likely remains bound to $CF_1\gamma$ even in its non-inhibitory conformation (Kato *et al.*, 1997), we also included $CF_1\varepsilon$ in our model. The model predicts that PGR5

may slot between the $CF_1\gamma$, $CF_1\alpha$, and $CF_1\beta$ subunits in a way that possibly hinders the rotation of $CF_1\gamma$ (Fig. 7b). Moreover, an Alphafold2 Multimer model predicts that SynPgr5 can bind to the $F_1\gamma$ subunit of the *Synechocystis* ATP synthase (Fig. 7c). We analysed the $SoCF_1\gamma$ / AtPGR5 (Supplementary Table S8) as well as SynF1γ / SynPgr5 (Supplementary Table S9) interaction interfaces using PDBePISA. Finally, we aligned the *Synechocystis* F_1y sequences against the sequence from *Synechococcus elongatus* sp. PCC 7942, which does not have an PGR5 ortholog. Out of the residues mediating predicted hydrogen bonds with SynPgr5, only Pro 2 in the *Synechocystis* F1γ sequence is not conserved in the *Synechococcus* sequence (Supplementary Table S10). Therefore, further work is required to fully elucidate the molecular details of the mechanism of PGR5 interaction with ATP synthase.

DISCUSSION

Substantial adjustments of thylakoid conductivity take place during sudden changes in light intensity in both chloroplasts and cyanobacteria, in order to control induction of the photoprotective mechanisms. Results shown herein indicate that this regulation is independent of the thiol redox state of $CF_1\gamma$ (Fig. 1), but dependent on another redox-based mechanism that involves the PGR5 protein in a manner that has been conserved in evolution from free-living cyanobacteria to green algae and C_3 plants, as well as C_4 plants.

Does PGR5 have a role in CET?

The PGR5 protein was originally understood to either directly catalyse or facilitate CET around PSI in plants (Munekage *et al.*, 2002) and cyanobacteria (Yeremenko *et al.*, 2005). Lack of PGR5 caused a distinct inability to oxidise PSI in chloroplasts, which was interpreted as being caused by failure to induce photosynthetic control and NPQ due to insufficient acidification of the thylakoid lumen in the absence of PGR5-mediated CET (Yamamoto & Shikanai, 2019). However, contrasting evidence was already provided early on showing that ferredoxin-dependent CET does function in the absence of PGR5 (Nandha *et al.*, 2007), suggesting that the phenotype of the *pgr5* mutant may be caused by another mechanism.

We showed previously that in *pgr5 Arabidopsis* plants overexpressing the chloroplast NADPH-dependent thioredoxin reductase (OE-NTRC *pgr5*), *pmf* was restored to a WT-level during LL-to-HL transitions (Nikkanen *et al.*, 2018). This was insufficient however, to induce photosynthetic control, resulting in the OE-NTRC *pgr5* plants suffering from almost as severe over-reduction of the electron transport chain as *pgr5* plants. Concurring results were more recently reported from *Arabidopsis pgr5*

cgl160 double mutants as well as plants expressing Plastid terminal oxidase 2 from *Chlamydomonas reinhardtii* (CrPTOX2) in the *pgr5* mutant background. Additional deletion of the ATP synthase assembly factor CGL160 resulted in a diminished amount of ATP synthase, limiting proton conductivity of the thylakoid membrane and allowing the *pgr5* mutant to maintain a WT-like *pmf* while still suffering from extreme acceptor side limitation of PSI (Kappel *et al.*, 2023). Similarly, the introduction of CrPTOX2 in *pgr5* background resulted in restoration of WT-like (ΔpH-dependent) NPQ, but oxidation of PSI was still as impaired as in *pgr5* mutants (Zhou *et al.*, 2023). These results suggest that the inability of *pgr5* mutants to induce photosynthetic control in HL is not simply caused by loss of ΔpH, but the AtPGR5 protein is directly required. It has been suggested that reduction of a disulphide in the Rieske subunit of Cyt b_6f could upregulate photosynthetic control by causing a conformational change that allows protonation of the His128 residue at a higher lumenal pH (Hald *et al.*, 2008; Degen & Johnson, 2024). Moreover, ΔpH-independent metabolic induction of photosynthetic control in *Chlamydomonas* was recently proposed by (Saroussi *et al.*, 2023). It remains to be investigated how these potential mechanisms may be affected in PGR5-deficient lines, but as NTRC overexpression results in stronger reduction of chloroplast TRX systems and redox regulated proteins (Nikkanen *et al.*, 2016), one could expect the activation of photosynthetic control in OE-NTRC *pgr5* to occur already at a lower ΔpH instead of being impaired.

Instead, the inability of *pgr5* mutants to oxidise PSI despite restoration of *pmf* generation may be explained by the presence of a partially photoinhibited PSI population with damaged F_A and F_B FeS clusters, resulting in repulsion of ferredoxin from the thylakoid membrane (Tiwari et al., 2024). This means that the bottleneck of electron transport in *pgr5* likely forms already at P700 or alternatively, as suggested by Buchert et al., (2020) for *Chlamydomonas*, at the Cyt b_6f complex, and not at ferredoxin as would be expected if PGR5 was directly involved in ferredoxin-dependent CET. Accordingly, our near-infrared spectroscopy measurements showed that both reduction and re-oxidation kinetics of Fed are delayed in *pgr5* under far-red light while PC was more strongly oxidised (Supplementary Fig. S5). This indicated that the bottleneck is not in electron transfer onwards from Fed, but the accumulation of damaged PSI centres would make it appear as if the mechanism of ferredoxin-dependent CET is impaired. These results suggest that the phenotype of *pgr5* mutants may not be caused by direct impairment of CET, but it must be noted that we cannot fully exclude that possibility since impairment of CET and ATP synthase deregulation could both theoretically result in the original FeS cluster damage. Interestingly, the PSI oxidation phenotype of *pgr5* could be rescued via expression of *Physcomitrium patens* flavodiiron proteins in Arabidopsis *pgr5* background (Yamamoto *et al.*, 2016), which likely provided a strong enough exogenous sink for electrons from ferredoxin to prevent PSI photodamage.

Finally, as it has been reported that a lack of CrPGR5 resulted in inefficient operation of the Q cycle (Buchert et al., 2020), it could be that the elevated gH+ values in *pgr5* mutants derive from diminished electrogenic activity of the Q cycle during the dark intervals where the rate of ECS signal decay is monitored. However, the post-illumination re-reduction rate of Cyt *f* was unimpaired in Arabidopsis *pgr5* (Supplementary Fig. S4). Moreover, Buchert et al. only detected a lower Cyt *f* re-reduction rate in anoxic *Chlamydomonas pgr5* samples. Therefore, it is unlikely that the elevated gH+ values in *pgr5* mutants are caused by impaired Q cycle activity.

The *Synechocystis* Δ*pgr5* mutant showed no impairment of CET (Fig. 2h). Our data is in line with a study by Miller et al. showing that the antimycin a-sensitive pathway (=PGR5-dependent) does not contribute to *pmf* formation during dark/light transitions in *Synechocystis*. Instead, the CET-dependent fraction of *pmf* generation was entirely attributable to the NDH-1 complex (Miller *et al.*, 2021). As the extra ATP produced by CET is understood to enable more efficient operation of the CBC by adjusting the ATP:NADPH ratio, the fact that no impairment of CO_2 fixation rate was observed in Δ*pgr5* (Supplementary Fig. S11e) further indicates that SynPgr5 is not needed for CET in *Synechocystis.* We propose it functions instead in reversible redox-dependent inhibition of ATP synthase.

Our ECS results both with the *Chlamydomonas pgr5* mutant (Fig. 3c) as well as the *pgr5-Cas Arabidopsis* mutant (Supplementary Fig. S6c) showed elevated proton flux (v_H+) in HL, which is also incompatible with a significant role for PGR5 in CET, and may rather indicate enhancement of the CET rate. Accordingly, CrPGR5 was not detected in CET supercomplexes (Iwai *et al.*, 2010). Recruitment of FNR to thylakoid membranes was reported to be diminished in the absence of CrPGR5 (Mosebach *et al.*, 2017), but a later study concluded that FNR remains associated with the thylakoids at all times (Kramer *et al.*, 2021). It was also recently speculated, based on simultaneous near-infrared and chlorophyll fluorescence spectroscopy, that the absence of AtPGR5 may in fact enhance CET activity in *Arabidopsis* (Maekawa *et al.*, 2024). A lower v_H+ in LL that cannot be fully explained by a lower linear electron transport rate has, however, been reported in *Arabidopsis* (Degen *et al.*, 2023) and *S. viridis* (Woodford *et al.*, 2024) *pgr5* mutants. Interestingly though, the *Arabidopsis pgr5-Cas* mutant showed WT-like v_H+ in LL (Supplementary Fig. S6c), suggesting that the low v_H+ in the *pgr5-1* mutant (Fig. 1c) may be affected by the additional mutation of the At2g1724 gene (Wada *et al.*, 2021). Moreover, in the fluctuating light conditions of the current study, no impairment of vH+ was detected in the *S. viridis pgr5* mutant (Supplementary Fig. S14c). It should be noted, however, that the presence of damaged PSI centres in *pgr5* mutants would result in a decrease in the ECS signal induced by a single-turnover flash (ECS_{ST}), which was used to normalise the ECS values in plant and algal samples. If this decrease in ECS_{ST} is not proportional to a decrease in the actinic light-induced ECS signal, it may result in overestimation of the *pmf* and vH+ parameters. However, normalisation of the *Chlamydomonas* ECS data (Fig. 3) to [Chl] only did not

eliminate the differences between WT and *pgr5* (Supplementary Fig. S13), suggesting that no major artefact is caused by potential PSI damage in *pgr5*.

Conserved PGR5-mediated regulatory mechanism of ATP synthase depends on thiol redox conditions

The g_H+ values elevated independently of *pmf* in PGR5-deficient *Synechocystis*, *Chlamydomonas*, *Arabidopsis*, and *S. viridis* during high-light phases of fluctuating light (Fig. 1–4, Supplementary Fig. S14) are consistent with PGR5 functioning as a direct or indirect down-regulator of ATP synthase activity (Tikkanen *et al.*, 2015; Kanazawa *et al.*, 2017; Nikkanen *et al.*, 2018). *In planta* interaction of AtPGR5 with $AtCF_1\gamma$ in BiFC tests (Fig. 7a) and *in silico* modelling of PGR5-$CF_1\gamma$ interaction complexes (Fig. 7b–c) suggest that PGR5 may inhibit ATP synthase by directly binding to the $F_1\gamma$ subunit. $F_1\varepsilon$-inhibition likely prevents ATP hydrolysis in dark and LL conditions, when *pmf* is low, while PGR5 would limit ATP synthase activity in HL, possibly allowed by the non-inhibitory "down" conformation of $F_1\varepsilon$ (Feniouk *et al.*, 2010), to allow build-up of sufficient ΔpH for induction of photoprotection.

The mechanism PGR5-dependent inhibition of ATP synthase activity may be regulated by the thiol redox state of the chloroplast stroma or cell. PGR5 contains a conserved cysteine residue (Munekage *et al.*, 2002; Yeremenko *et al.*, 2005), which could be target for regulatory thiol modifications. In line with this hypothesis, AtPGR5 was found able to interact with AtNTRC in an *in planta* BiFC test, and overexpression of AtNTRC resulted in intensified downregulation of thylakoid proton conductivity during transitions to HL, but only in the presence of AtPGR5 (Nikkanen *et al.*, 2018). Moreover, using a *pgr5 ntrc* double mutant of *Arabidopsis*, Naranjo et al. showed that the high NPQ observed in *ntrc* mutant plants is dependent on the presence of AtPGR5 (Naranjo *et al.*, 2021). *Ntrc* mutant plants have a diminished AtPGR5 protein level (Nikkanen *et al.*, 2018), most likely to compensate for the impaired activation of ATP synthase via reduction of the $AtCF_1\gamma$ disulphide (Carrillo *et al.*, 2016; Nikkanen *et al.*, 2016).

The *pgr5* mutation could, hypothetically, result in the chloroplast thioredoxin systems themselves becoming more oxidised or reduced, which would affect the redox state and activity of some other inhibitory factor of ATP synthase. However, no differences were reported between Arabidopsis WT and *pgr5* in the vivo redox states of redox regulated CBC enzymes FBPase and SBPase, of NADP-malate dehydrogenase, or of $CF_1\gamma$ (Okegawa & Motohashi, 2020) (Fig 1g). These findings indicate that altered activity of the thioredoxin systems is not a major factor in the gH+ phenotype of *pgr5*. A small population of reduced $CF_1\gamma$ was detected in *pgr5* in the dark (Fig. 1g), but this would not affect the gH+ dynamics under fluctuating light apart from the very first seconds of the dark-to-light transition.

It has been suggested that a disulphide bridge between AtPGR5 and AtPGRL1 is required for PGR5/PGRL1-dependent CET in *Arabidopsis* (Hertle *et al.*, 2013). More recently, however, a model was proposed where the function of AtPGRL1 is to stabilise AtPGR5 (Rühle *et al*., 2021). Moreover, *Chlamydomonas* PGR5 with the conserved cysteine residue mutated to a serine was able to complement the impairment of CET in the *Chlamydomonas pgr5* mutant (Buchert *et al.*, 2020), suggesting that the conserved cysteine residue in PGR5 may be involved in a non-CET related regulatory mechanism.

Transient reduction of AtPGRL1 occurs upon onset of illumination, coinciding with increase in *pmf*, PSI oxidation, and induction of NPQ (Hertle *et al.*, 2013; Nikkanen *et al.*, 2018; Wolf *et al.*, 2020; Chaturvedi *et al.*, 2024). TRXm4 forms a disulphide bridge with AtPGRL1, and cleavage of that disulphide (most likely by another thioredoxin isoform) and transient release of TRXm4 also occur at dark-to-light transitions (Okegawa & Motohashi, 2020). This has been suggested to indicate activation of CET (Hertle *et al.*, 2013; Wolf *et al.*, 2020; Okegawa & Motohashi, 2020; Chaturvedi *et al.*, 2024), but the same results could also be interpreted as reduction of AtPGRL1 affecting the association of AtPGR5 with AtPGRL1, releasing AtPGR5 to interact with ATP synthase and to downregulate its activity (Fig. 8). This would limit H^+ efflux from the lumen and cause build-up of *pmf*, and consequently, induction of NPQ and photosynthetic control. As recently proposed for *S. viridis* (Nix *et al.*, 2024), PGR5 may be bound to PGRL1 homodimers that are held together by an intermolecular disulphide between the Cys 116 residues of the monomers, possibly maintained by a bound TRXm4. Once stromal redox regulatory systems become sufficiently reduced, the disulphide would be reduced, potentially by another TRX isoform, dissolving the PGRL1 dimer and releasing PGR5.

We therefore suggest that the phenotypes of *pgr5* mutants may have been misinterpreted as being caused by directly impaired CET. For example, it was recently shown that point mutations of disulphide-forming cysteine residues in AtPGRL1a results in elevated *pmf*, NPQ, and donor-side limitation of PSI (Chaturvedi *et al.*, 2024). While the authors did not show data on g_H+, it is possible that this phenotype was caused not by increased CET, but by constitutive inhibition of ATP synthase activity by AtPGR5. Similarly, it has been reported that AtPGR5 can enhance CET if both AtPGRL1 and AtPGRL2, a protein causing degradation of AtPGR5 in the absence of AtPGRL1, are missing (Rühle et al., 2021). This conclusion was based on higher *pmf* and NPQ in the *pgrl1a pgrl1b pgrl2* triple mutant compared to *pgrl1* or *pgr5* single mutants. We suggest, however, that the increased *pmf* was, again, probably mediated or at least contributed to by lowered ATP synthase conductivity.

In the current study, we explored the effects of perturbing the chloroplast or cellular redox state on the conductivity of ATP synthase. Interestingly, we found that addition of methyl viologen (MV) results, either directly or e.g. via affecting the TrxL2-dependent oxidative pathway (Yoshida *et al.*, 2018), in

strong reduction of chloroplast enzymes in *Arabidopsis*, including $AtCF_1\gamma$ (Fig. 5a). While we cannot fully exclude the possibility of the apparent reduction of chloroplast enzymes in presence of MV being caused by overoxidation of thiols to sulphenic acids (Huang *et al.*, 2019), the elevation of g_H+ at the onset of illumination in MV-treated leaves (Fig. 5b) suggests otherwise, at least in the case of $CF_1\gamma$ in darkness. Moreover, overoxidation would inactivate 2-CysPrxs, preventing their oxidising effect on other thiol proteins in the chloroplast, (Pérez-Ruiz *et al.*, 2017; Vaseghi *et al.*, 2018). Thus, we conclude that MV treatment indeed results in strong reduction of chloroplast redox enzymes, including $AtCF_1\gamma$.

Accordingly, g_H+ was elevated in dark-adapted MV-treated leaves (Fig. 5b). However, strong downregulation of g_H+ during illumination was measured in MV-leaves, but only in the presence of AtPGR5 (Fig. 5c). Thiol-alkylating agent NEM had a similar albeit less dramatic effect (Fig. 6c). Interestingly, lack of AtPGR5 made the plants immune to NEM-induced g_H+ decrease under HL, but did not prevent the decrease observed under LL phases of the fluctuating light experiment. These results provide further evidence that AtPGR5 is required for redox-dependent downregulation of g_H+ under high irradiance, although it should be noted that we cannot exclude indirect effects of MV/NEM treatment interfering with metabolic regulation of ATP synthase (Kohzuma *et al.*, 2013). We hypothesise that in WT *Arabidopsis*, addition of MV likely causes strong reduction of either AtPGR5/AtPGRL1/AtTRXm4 directly or some associated factor that would, without an MV treatment, function as an inhibitor of the ATP synthase during sudden increases in light intensity. Importantly, this inhibitory effect overrides the activating effect of a fully reduced $AtCF_1\gamma$. In the absence of AtPGR5, the inhibitory mechanism does not function even in presence of MV.

In *Synechocystis*, addition of NEM caused an opposite phenotype to *Arabidopsis*, with g_H+ being elevated rather than diminished (Fig. 6a). The NEM-induced g_H+ increase was diminished in *Synechocystis Δpgr5* and absent in WT *Synechococcus*, a species that does not have a PGR5 orthologue (Shimakawa *et al.*, 2016). Untreated *Synechococcus* did, however, exhibit similar downregulation of g_H+ under strong illumination as *Synechocystis* or *Arabidopsis* (Supplementary Fig. S12). These results suggest that the regulatory mechanisms involved in this response may differ between organisms in terms of directionality of redox-regulation and involvement of PGR5, with *Synechococcus* possibly using an unrelated, convergently evolved analogous mechanism. The molecular details of these differing responses remain to be elucidated in future studies.

Interestingly, it has been reported that alkylation of cysteine 89 (Cys 130 in the full sequence containing the transit peptide) in the (*Spinacia oleracea*) $SoCF_1\gamma$ by NEM or crosslinking Cys89 with Cys322 inhibits photophosphorylation and induces loss of the proton gradient (McCarty & Fagan, 1973; Soteropoulos *et al.*, 1994; Evron & Pick, 1997). This effect was not observed in the dark, suggesting Cys89 only becomes accessible to modifications in light upon generation of ΔpH (McCarty

& Fagan, 1973). It is therefore possible that Cys89 is responsible for the middle band in the $AtCF_1\gamma$ mobility shift assays that is also present in the control sample (Fig. 1e), where all thiols accessible in the dark are alkylated with NEM before addition of MAL-PEG. MAL-PEG likely gains access to Cys89 after the subsequent DTT treatment, resulting in the observed mobility shift. The $F_1\gamma$ Cys89 residue is conserved in the green lineage, including cyanobacteria (Hisabori *et al.*, 2013), suggesting a functional role. Our computational models of $AtCF_1\gamma$-AtPGR5 and $SynF_1\gamma$-SynPgr5 interaction complexes predict, however, that neither the conserved Cys30 in SynPgr5, or Cys90 in $SynF_1\gamma$ are involved in mediating the protein–protein interactions (Supplementary Tables S1, S2). This is also consistent with the lack of changes in $AtCF_1\gamma$ redox state in fluctuating light (Fig. 1f–g), suggesting that thiol/disulphide exchanges of $F_1\gamma$ are not involved in the mechanism of adjusting g_H+ in fluctuating light. The predicted binding of SynPgr5 to $SynF_1\gamma$ in our model somewhat resembles the binding of the inhibitory IF_1 protein to mitochondrial ATP synthase, which slots between the $F_1\gamma$, $F_1\alpha$, and $F_1\beta$ subunits (García-Bermúdez & Cuezva, 2016). This could also explain the observed interaction between cucumber PGR5 and $F_1\beta$ (Wu et al., 2021).

An alternative or additional mechanism for the regulation of g_H+ in fluctuating light in plants could function through changes in intercellular inorganic carbon concentration (C_i). C_i increases upon HL to LL transitions as carbon fixation rate suddenly drops (Vialet-Chabrand *et al.*, 2017), and increase in C_i is known to increase g_H+ via an unknown regulatory pathway (Kohzuma *et al.*, 2013). It is unlikely, however, that the inability of *pgr5* to down-regulate g_H+ in HL would be caused by an elevated concentration of C_i, because WT-like levels of C_i as well as CO_2 fixation rates were measured under HL in PGR5-deficient rice plants (Nishikawa *et al.*, 2012; Wada *et al.*, 2018). The carbon fixation capacity of *pgr5* plants only goes down as a consequence of prolonged HL exposure and ensuing PSI photoinhibition (Gollan *et al.*, 2017; Lima-Melo *et al.*, 2018). Similarly, we detected no impairment of CO_2 fixation in the *Synechocystis* Δ*pgr5* mutant (Supplementary Fig. S11e). Thus, it is also unlikely that the elevated gH+ in PGR5-deficient plants or cyanobacteria would be caused by an excess of P_i due to a hyperactivated CBC. Interestingly, expression of FlvA and FlvB from the moss *Physcomitrium patens* in the Arabidopsis *pgr5* mutant background alleviated the elevated g_H+ phenotype (Yamamoto & Shikanai, 2020), highlighting the complex relationship between oxidation of PSI and regulation of ATP synthase.

Physiological significance of PGR5-mediated downregulation of ATP synthase in *Synechocystis*

Lack of SynPgr5 caused no impairment of PSI oxidation or growth despite lowered *pmf* in *Synechocystis* under fluctuating light (Fig. 2). This may be due to prevalence of FDPs as a protective electron sink on the acceptor side of PSI in cyanobacteria (Allahverdiyeva *et al.*, 2013; Santana-

Sanchez *et al.*, 2019). Slightly elevated FDP activity was indeed measured in fluctuating light grown Δ*pgr5* under fluctuating light (Fig. 2i), which may allow the mutant to maintain sufficient PSI oxidation in HL despite diminished *pmf* and to grow similarly to WT in fluctuating light (Fig. 2g). We have recently proposed that dissipation of *pmf* (lower cytosolic pH) causes FDP hetero-oligomers to associate more strongly with the thylakoid membrane, increasing photoprotective O_2 photoreduction activity (Eckardt *et al.*, 2024; Nikkanen *et al.*, 2025). In Δ*pgr5*, the decreased *pmf* due to elevated g_H+ in HL (Fig. 2a–b) may therefore cause the slightly increased FDP activity during the HL phases of fluctuating light conditions (Fig. 2i), at least partly compensating for the loss of photoprotective capacity via ΔpH-induced photosynthetic control. Even in the absence of Flv1/3-mediated O_2 photoreduction in the Δ*pgr5 flv3* double mutant, however, no significant additional impairment of PSI oxidation in comparison to Δ*flv3* single mutant was observed (Fig. 2e–f). The lack of any clear effect on PSI oxidation in *Δpgr5* is thus most likely explained by PSI/PSII stoichiometry, as *Synechocystis* harbours 2-to-5-fold more PSI than PSII complexes (Moore & Vermaas, 2024).

Interestingly, there appears to be a regulatory link between FDPs, ATP synthase, and SynPgr5 in cyanobacteria. During transitions to HL, lack of Flv1/3 results in a loss up to 75% of the proton flux during the first minute of illumination in *Synechocystis* (Nikkanen *et al.*, 2020) (Fig. 2c) as well as in the filamentous model cyanobacterium *Anabaena* sp. PCC 7120 (Santana-Sánchez *et al.*, 2023). However, cyanobacterial cells compensate for this by downregulating g_H+ (Fig. 2a), achieving WT-like *pmf* levels after the initial stages of HL transitions (Fig. 2b). In in the absence of both Flv1/3 and SynPgr5 in the *Δpgr5 flv3* double mutant, however, this downregulation of g_H+ did not occur, indicating that SynPgr5-mediated inhibition of ATP-synthase is required for the compensatory mechanism. Interestingly, proton flux also recovered to WT-levels in *Δpgr5 flv3* (Fig. 2c), suggesting e.g. increased CET via NDH-1.

It remains to be investigated what the environmental conditions are where SynPgr5 has a physiologically significant role. Future studies should focus for example on mixotrophic conditions, where overexpression of SynPgr5 has been shown to inhibit growth (Margulis *et al.*, 2020) and diurnal rhythms, which present additional challenges for coordination of the bioenergetic pathways and metabolism in cyanobacteria (Solymosi *et al.*, 2020; Ortega-Martínez *et al.*, 2024).

Conclusion

The activity of chloroplast or cyanobacterial ATP synthase is dynamically regulated during fluctuations in light intensity. These adjustments are not dependent on the thiol redox state of the $F_1\gamma$ subunit, but instead depend on the PGR5 protein as well as the thiol redox state of the stroma or

cytosol. This mechanism has been conserved in evolution from free-living cyanobacteria to chloroplasts in algae, C_3 plants as well as C_4 plants. The inability to downregulate ATP synthase activity under strong illumination is the only phenotype of PGR5-deficient knockout mutants that can be observed in all representatives of the groups of photosynthetic organisms studied here; cyanobacterium *Synechocystis* sp. PCC 6803, green alga *Chlamydomonas reinhardtii*, C_3 plant *Arabidopsis thaliana*, and C_4 plant *Setaria viridis*. The role of PGR5 is vital for oxidation of PSI in plants and algae, but not in cyanobacteria. We also demonstrated that the cyanobacterial Pgr5 is not needed for cyclic electron transport. We suggest that PGR5 directly binds to ATP synthase and functions as an inhibitory factor in a manner that is dependent on the thiol redox state of the cell or chloroplast. The observed effect of plant PGR5 on CET is likely an indirect consequence of misregulation of ATP synthase and, as shown by (Tiwari *et al.*, 2024), increased photoinhibition of PSI, although a role for PGR5 in regulating CET via Cyt b_6f cannot be excluded (Buchert *et al.*, 2020). Our study lays important groundwork for understanding the regulatory mechanisms of the *pmf* and their evolution, possibly enabling biotechnologies to modulate *pmf* regulation for enhancement of photosynthetic efficiency in crop plants or microbial bioproduction platforms.

Supplementary Data

Fig. S1. PCR analysis to verify full segregation of the Δ*pgr5* and Δ*pgr5 flv3* strains.,

Fig. S2. Mobility shift assay of the in vivo thiol redox state of CBC enzyme fructose 1,6 bisphosphatase (FBPase).

Fig. S3. PSI quantum yield in PGR5-mutants of Arabidopsis and *Synechocystis*.

Fig. S4. Cytochrome *f* post-illumination re-reduction rates in Arabidopsis WT and *pgr5-1* mutant leaves.

Fig. S5. Redox kinetics of PC, P700, and Fed upon a pulse of far-red light in Arabidopsis WT and *pgr5*.

Fig. S6. *Pmf* dynamics in the *Arabidopsis thaliana* WT and *pgr5-Cas* mutant in fluctuating light.

Fig. S7. *Pmf* dynamics in the *Arabidopsis thaliana* WT and *pgr5*-Cas mutant in fluctuating light in the presence of inhibitors of mitochondrial respiration

Fig. S8. Immunodetection of AtpB and Flv3 levels in *Synechocystis* strains.

Fig. S9. *In vivo* redox kinetics of P700, PC, and Fed and O_2 and CO_2 gas exchange in *Δpgr5 flv3* and Δ*flv3* strains of *Synechocystis*.

Fig. S10. P700 oxidation under far-red light in WT and Δ*pgr5* strains of *Synechocystis*.

Fig. S11. Photosynthetic phenotype of the *Synechocystis Δpgr5* strain.

Fig. S12. *Pmf* dynamics in *Synechococcus elongatus* sp. PCC 7942 under fluctuating light.

Fig, S13. *Pmf* and vH+ dynamics in *Chlamydomonas reinhardtii* under fluctuating light without ECS_{ST} normalisation.

Fig. S14. *Pmf* dynamics in the C_4 model grass *Setaria viridis.*

Fig. S15. Effect of methyl viologen on thylakoid conductivity in *Synechocystis*.

Fig. S16. Effect of N-ethylmaleimide (NEM) on thylakoid conductivity under fluctuating light in Arabidopsis.

Fig. S17. Negative controls for the BiFC tests.

Fig. S18. Positive controls for bimolecular fluorescence com

plementation (BiFC) tests.

Table S1. LMEM report table for Arabidopsis WT vs *pgr5-1* (full data).

Table S2. LMEM report table for Arabidopsis WT vs *pgr5-1* (high light data).

Table S3. LMEM report table for Arabidopsis WT vs *pgr5*-Cas (full data).

Table S4. LMEM report table for Arabidopsis WT vs *pgr5*-Cas (high light only).

Table S5. LMEM report table for *Chlamydomonas* WT vs *pgr5* (full data).

Table S6. LMEM report table for *Setaria viridis* WT vs *pgr5-1* (full data).

Table S7. LMEM report table for *Synechocystis* WT vs Δ*pgr5* (full data).

Table S8. Hydrogen Bond Interactions and salt bridges between AtPGR5 and $SoCF_1\gamma$ in the ClusPro 2.0 docking model.

Table S9. Hydrogen Bond Interactions between $SynCF_1\gamma$ and SynPgr5 in the AlphaFold2 model.

Table S10. Alignment of the ATP synthase F1γ amino acid sequences from Synechocystis sp. PCC 6803 and Synechococcus elongatus sp. PCC 7942

Acknowledgements

We thank Drs Martina Jokel and Arjun Tiwari for providing *Chlamydomonas* strains and the Arabidopsis *pgr5*-Cas line, respectively. Linda Nevala, Mahfuzur Rahman, Iida Turpeinen, and Tapio Ronkainen are thanked for technical assistance, and the Turku Bioscience CIC Imaging Core for imaging infrastructure and assistance.

Author Contributions

L.N. conceived the research idea, devised the experimental plan, performed most of the experiments, analysed the data, and wrote the first draft of the article. L.T.W. performed part of the cyanobacterial ECS and Dual-KLAS-NIR measurements and analysed the data. R.W. and M.E. performed the ECS measurements in *S. viridis*. H.M. created the *Synechocystis* Δ*pgr5* and Δ*pgr5 flv3* mutants. D.K. performed *Chlamydomonas* cell culture and ECS measurements. E.R. and Y.A. supervised research and provided resources. All authors participated in editing the article.

Conflicts of interest

The authors declare no conflicts of interest.

Funding

This work was supported by the Research Council of Finland grants #354876 (to L.N.), #315119 (to Y.A.), and # 276392 (to E.R.), funding from Jane and Aatos Erkko Foundation (to E.R.), Novo Nordisk Foundation grants NNF20OC0064371 (PhotoCat, to Y.A.) and NNF22OCOO79717 (Photo-e-Microbes, to L.T.W.) as well as Australian Research Council 's Discovery Project (DP230100175) and the Thomas Davies Research Grant for Marine, Soil and Plant Biology from the Australian Academy of Sciences (to M.E.).

Data Availability

The SynPgr5/SynCF1γ AlphaFold2 multimer model is available in the ModelArchive database at https://www.modelarchive.org/doi/10.5452/ma-v9v6q. All relevant data generated in this study are included in this paper and its Supplementary Data.

References

Akiyama K, Ozawa S-I, Takahashi Y, Yoshida K, Suzuki T, Kondo K, Wakabayashi K, Hisabori T. **2023**. Two specific domains of the γ subunit of chloroplast F_oF_1 provide redox regulation of the ATP synthesis through conformational changes. *Proceedings of the National Academy of Sciences* **120**.

Allahverdiyeva Y, Mustila H, Ermakova M, Bersanini L, Richaud P, Ajlani G, Battchikova N, Cournac L, Aro E-M. **2013**. Flavodiiron proteins Flv1 and Flv3 enable cyanobacterial growth and photosynthesis under fluctuating light. *Proceedings of the National Academy of Sciences of the United States of America* **110**: 4111–4116.

Armbruster U, Carrillo LR, Venema K, Pavlovic L, Schmidtmann E, Kornfeld A, Jahns P, Berry JA, Kramer DM, Jonikas MC. **2014**. Ion antiport accelerates photosynthetic acclimation in fluctuating light environments. *Nature Communications* **5**: 5439.

Armbruster U, Correa Galvis V, Kunz HH, Strand DD. **2017**. The regulation of the chloroplast proton motive force plays a key role for photosynthesis in fluctuating light. *Current opinion in plant biology* **37**: 56–62.

Avenson TJ, Cruz JA, Kanazawa A, Kramer DM. **2005**. Regulating the proton budget of higher plant photosynthesis. *Proceedings of the National Academy of Sciences of the United States of America* **102**: 9709–9713.

Bailleul B, Cardol P, Breyton C, Finazzi G. **2010**. Electrochromism: a useful probe to study algal photosynthesis. *Photosynthesis Research* **106**: 179–189.

Balmer Y, Vensel WH, Hurkman WJ, Buchanan BB. **2006**. Thioredoxin target proteins in chloroplast thylakoid membranes. *Antioxidants & Redox Signaling* **8**: 1829–1834.

von Bismarck T, Korkmaz K, Ruß J, Skurk K, Kaiser E, Correa Galvis V, Cruz JA, Strand DD, Köhl K, Eirich J, *et al.* 2023. Light acclimation interacts with thylakoid ion transport to govern the dynamics of photosynthesis in Arabidopsis. *New Phytologist* **237**: 160–176.

Buchert F, Bailleul B, Joliot P. **2021**. Disentangling chloroplast ATP synthase regulation by proton motive force and thiol modulation in Arabidopsis leaves. *Biochimica et Biophysica Acta (BBA) - Bioenergetics* **1862**: 148434.

Buchert F, Mosebach L, Gäbelein P, Hippler M. **2020**. PGR5 is required for efficient Q cycle in the cytochrome b6f complex during cyclic electron flow. *The Biochemical journal* **477**: 1631–1650.

Carrillo LR, Froehlich JE, Cruz JA, Savage LJ, Kramer DM. **2016**. Multi-level regulation of the chloroplast ATP synthase: the chloroplast NADPH thioredoxin reductase C (NTRC) is required for redox modulation specifically under low irradiance. *Plant Journal* **87**: 654–663.

Chaturvedi AK, Dym O, Levin Y, Fluhr R. **2024**. PGR5-LIKE PHOTOSYNTHETIC PHENOTYPE1A redox states alleviate photoinhibition during changes in light intensity. *Plant Physiology* **194**: 1059–1074.

1026 **Checchetto V, Segalla A, Allorent G, La Rocca N, Leanza L, Giacometti GM, Uozumi N, Finazzi G,**
1027 **Bergantino E, Szabò I**. **2012**. Thylakoid potassium channel is required for efficient photosynthesis in
1028 cyanobacteria. *Proceedings of the National Academy of Sciences* **109**: 11043–11048.

1029 **Cobley J, Noble A, Bessell R, Guille M, Husi H**. **2020**. Reversible Thiol Oxidation Inhibits the
1030 Mitochondrial ATP Synthase in Xenopus laevis Oocytes. *Antioxidants* **9**: 215.

1031 **Cruz JA, Avenson TJ, Kanazawa A, Takizawa K, Edwards GE, Kramer DM**. **2005**. Plasticity in light
1032 reactions of photosynthesis for energy production and photoprotection. *Journal of experimental*
1033 *botany* **56**: 395–406.

1034 **Cruz JA, Sacksteder CA, Kanazawa A, Kramer DM**. **2001**. Contribution of electric field (Delta psi) to
1035 steady-state transthylakoid proton motive force (pmf) in vitro and in vivo. Control of pmf parsing
1036 into Delta psi and Delta pH by ionic strength. *Biochemistry* **40**: 1226–1237.

1037 **DalCorso G, Pesaresi P, Masiero S, Aseeva E, Schuenemann D, Finazzi G, Joliot P, Barbato R, Leister**
1038 **D**. **2008**. A complex containing PGRL1 and PGR5 is involved in the switch between linear and cyclic
1039 electron flow in Arabidopsis. *Cell* **132**: 273–285.

1040 **Dann M, Leister D**. **2019**. Evidence that cyanobacterial Sll1217 functions analogously to PGRL1 in
1041 enhancing PGR5-dependent cyclic electron flow. *Nature Communications* **10**: 5299.

1042 **Davis GA, Kanazawa A, Schoettler MA, Kohzuma K, Froehlich JE, Rutherford AW, Satoh-Cruz M,**
1043 **Minhas D, Tietz S, Dhingra A, *et al.* 2016**. Limitations to photosynthesis by proton motive force-
1044 induced photosystem II photodamage. *Elife* **5**: e16921.

1045 **Degen GE, Jackson PJ, Proctor MS, Zoulias N, Casson SA, Johnson MP**. **2023**. High cyclic electron
1046 transfer via the PGR5 pathway in the absence of photosynthetic control. *Plant Physiology* **192**: 370–
1047 386.

1048 **Degen GE, Johnson MP**. **2024**. Photosynthetic control at the cytochrome *b* 6 *f* complex. *The Plant*
1049 *Cell* **36**: 4065–4079.

1050 **Eckardt NA, Allahverdiyeva Y, Alvarez CE, Büchel C, Burlacot A, Cardona T, Chaloner E, Engel BD,**
1051 **Grossman AR, Harris D, *et al.* 2024**. Lighting the way: Compelling open questions in photosynthesis
1052 research. *The Plant Cell*.

1053 **Ermakova M, Woodford R, Fitzpatrick D, Nix SJ, Zwahlen SM, Farquhar GD, von Caemmerer S,**
1054 **Furbank RT**. **2024**. Chloroplast NADH dehydrogenase-like complex-mediated cyclic electron flow is
1055 the main electron transport route in <scp>C</scp> $_4$ bundle sheath cells. *New Phytologist* **243**: 2187–
1056 2200.

1057 **Evron Y, Pick U**. **1997**. Modification of Sulfhydryl Groups in the [gamma]-Subunit of Chloroplast-
1058 Coupling Factor 1 Affects the Proton Slip through the ATP Synthase. *Plant Physiology* **115**: 1549–
1059 1555.

1060 **Fan D-Y, Nie Q, Hope AB, Hillier W, Pogson BJ, Chow WS**. **2007**. Quantification of cyclic electron
1061 flow around Photosystem I in spinach leaves during photosynthetic induction. *Photosynthesis*
1062 *Research* **94**: 347–357.

Feniouk BA, Kato-Yamada Y, Yoshida M, Suzuki T. **2010**. Conformational Transitions of Subunit in ATP Synthase from Thermophilic Bacillus PS3. *Biophysical Journal* **98**: 434–442.

Feniouk BA, Suzuki T, Yoshida M. **2006**. The role of subunit epsilon in the catalysis and regulation of FOF1-ATP synthase. *Biochimica et Biophysica Acta (BBA) - Bioenergetics* **1757**: 326–338.

Foyer CH, Hanke G. **2022**. ROS production and signalling in chloroplasts: cornerstones and evolving concepts. *The Plant Journal* **111**: 642–661.

Fujii T, Yokoyama E, Inoue K, Sakurai H. **1990**. The sites of electron donation of Photosystem I to methyl viologen. *Biochimica et Biophysica Acta (BBA) - Bioenergetics* **1015**: 41–48.

García-Bermúdez J, Cuezva JM. **2016**. The ATPase Inhibitory Factor 1 (IF1): A master regulator of energy metabolism and of cell survival. *Biochimica et Biophysica Acta (BBA) - Bioenergetics* **1857**: 1167–1182.

Gollan PJ, Lima-Melo Y, Tiwari A, Tikkanen M, Aro E-M. **2017**. Interaction between photosynthetic electron transport and chloroplast sinks triggers protection and signalling important for plant productivity. *Philosophical Transactions of the Royal Society B: Biological Sciences* **372**.

Guinea Diaz M, Nikkanen L, Himanen K, Toivola J, Rintamäki E. **2020**. Two chloroplast thioredoxin systems differentially modulate photosynthesis in Arabidopsis depending on light intensity and leaf age. *Plant Journal* **104**.

Guo J, Nguyen AY, Dai Z, Su D, Gaffrey MJ, Moore RJ, Jacobs JM, Monroe ME, Smith RD, Koppenaal DW, *et al.* 2014. Proteome-wide light/dark modulation of thiol oxidation in cyanobacteria revealed by quantitative site-specific redox proteomics. *Molecular & cellular proteomics: MCP* **13**: 3270–3285.

Hahn A, Vonck J, Mills DJ, Meier T, Kühlbrandt W. **2018**. Structure, mechanism, and regulation of the chloroplast ATP synthase. *Science* **360**.

Hangarter RP, Good NE. **1982**. Energy Thresholds for Atp Synthesis in Chloroplasts. *Biochimica et biophysica acta* **681**: 397–404.

Helman Y, Tchernov D, Reinhold L, Shibata M, Ogawa T, Schwarz R, Ohad I, Kaplan A. **2003**. Genes encoding a-type flavoproteins are essential for photoreduction of O-2 in cyanobacteria. *Current Biology* **13**: 230–235.

Herdean A, Nziengui H, Zsiros O, Solymosi K, Garab G, Lundin B, Spetea C. **2016a**. The Arabidopsis Thylakoid Chloride Channel AtCLCe Functions in Chloride Homeostasis and Regulation of Photosynthetic Electron Transport. *Frontiers in Plant Science* **7**: 115.

Herdean A, Teardo E, Nilsson AK, Pfeil BE, Johansson ON, Unnep R, Nagy G, Zsiros O, Dana S, Solymosi K, *et al.* 2016b. A voltage-dependent chloride channel fine-tunes photosynthesis in plants. *Nature Communications* **7**: 11654.

1097 **Hertle AP, Blunder T, Wunder T, Pesaresi P, Pribil M, Armbruster U, Leister D**. **2013**. PGRL1 Is the
1098 Elusive Ferredoxin-Plastoquinone Reductase in Photosynthetic Cyclic Electron Flow. *Molecular cell*
1099 **49**: 511–523.

1100 **Hirasawa M, Tamura G**. **1980**. Ferredoxin-Dependent Nitrite Reductase from Spinach Leaves.
1101 *Agricultural and Biological Chemistry* **44**: 749–758.

1102 **Hisabori T, Sunamura E-I, Kim Y, Konno H**. **2013**. The Chloroplast ATP Synthase Features the
1103 Characteristic Redox Regulation Machinery. *Antioxidants & Redox Signaling* **19**: 1846–1854.

1104 **Huang J, Willems P, Wei B, Tian C, Ferreira RB, Bodra N, Gache SAM, Wahni K, Liu K, Vertommen D,**
1105 ***et al.*** **2019**. Mining for protein S-sulfenylation in Arabidopsis uncovers redox-sensitive sites.
1106 *Proceedings of the National Academy of Sciences of the United States of America* **116**: 21256–21261.

1107 **Hubáček M, Wey LT, Kourist R, Malihan-Yap L, Nikkanen L, Allahverdiyeva Y**. **2024**. Strong
1108 heterologous electron sink outcompetes alternative electron transport pathways in photosynthesis.
1109 *The Plant Journal*.

1110 **Ilik P, Pavlovic A, Kouril R, Alboresi A, Morosinotto T, Allahverdiyeva Y, Aro E-M, Yamamoto H,**
1111 **Shikanai T**. **2017**. Alternative electron transport mediated by flavodiiron proteins is operational in
1112 organisms from cyanobacteria up to gymnosperms. *New Phytologist* **214**: 967–972.

1113 **Imashimizu M, Bernat G, Sunamura E-I, Broekmans M, Konno H, Isato K, Roegner M, Hisabori T**.
1114 **2011**. Regulation of F0F1-ATPase from Synechocystis sp PCC 6803 by gamma and epsilon Subunits Is
1115 Significant for Light/Dark Adaptation. *Journal of Biological Chemistry* **286**: 26595–26602.

1116 **Iwai M, Takizawa K, Tokutsu R, Okamuro A, Takahashi Y, Minagawa J**. **2010**. Isolation of the elusive
1117 supercomplex that drives cyclic electron flow in photosynthesis. *Nature* **464**: 1210–1213.

1118 **Johnson X, Steinbeck J, Dent RM, Takahashi H, Richaud P, Ozawa S-I, Houille-Vernes L, Petroutsos**
1119 **D, Rappaport F, Grossman AR, *et al.* 2014**. Proton Gradient Regulation 5-Mediated Cyclic Electron
1120 Flow under ATP- or Redox-Limited Conditions: A Study of □ *ATPase pgr5* and □ *rbcL pgr5* Mutants in
1121 the Green Alga *Chlamydomonas reinhardtii* . *Plant Physiology* **165**: 438–452.

1122 **Jokel M, Johnson X, Peltier G, Aro E-M, Allahverdiyeva Y**. **2018**. Hunting the main player enabling
1123 Chlamydomonas reinhardtii growth under fluctuating light. *Plant Journal* **94**: 822–835.

1124 **Joliot P, Johnson GN**. **2011**. Regulation of cyclic and linear electron flow in higher plants.
1125 *Proceedings of the National Academy of Sciences of the United States of America* **108**: 13317–13322.

1126 **Kanazawa A, Kramer DM**. **2002**. In vivo modulation of nonphotochemical exciton quenching (NPQ)
1127 by regulation of the chloroplast ATP synthase. *Proceedings of the National Academy of Sciences of*
1128 *the United States of America* **99**: 12789–12794.

1129 **Kanazawa A, Ostendorf E, Kohzuma K, Hoh D, Strand DD, Sato-Cruz M, Savage L, Cruz JA, Fisher N,**
1130 **Froehlich JE, *et al.* 2017**. Chloroplast ATP Synthase Modulation of the Thylakoid Proton Motive
1131 Force: Implications for Photosystem I and Photosystem II Photoprotection. *Frontiers in Plant Science*
1132 **8**: 719.

1133 **Kappel S, Thiele W, Gefen-Treves S, Henze A, Armbruster U, Schöttler MA**. **2023**. A congestion
1134 downstream of PSI causes the over-reduction of the electron transport chain in *pgr5* independent of
1135 membrane energization. *bioRxiv*.

1136 **Kato Y, Matsui T, Tanaka N, Muneyuki E, Hisabori T, Yoshida M**. **1997**. Thermophilic F1-ATPase Is
1137 Activated without Dissociation of an Endogenous Inhibitor, ε Subunit. *Journal of Biological Chemistry*
1138 **272**: 24906–24912.

1139 **Kiirats O, Cruz JA, Edwards GE, Kramer DM**. **2009**. Feedback limitation of photosynthesis at high
1140 CO2 acts by modulating the activity of the chloroplast ATP synthase. *Functional Plant Biology* **36**:
1141 893–901.

1142 **Klughammer C, Schreiber U**. **2008**. Saturation Pulse method for assessment of energy conversion in
1143 PSI. *PAM Application Notes* **1**: 11–14.

1144 **Klughammer C, Schreiber U**. **2016**. Deconvolution of ferredoxin, plastocyanin, and P700
1145 transmittance changes in intact leaves with a new type of kinetic LED array spectrophotometer.
1146 *Photosynthesis Research* **128**: 195–214.

1147 **Kohzuma K, Dal Bosco C, Meurer J, Kramer DM**. **2013**. Light- and Metabolism-related Regulation of
1148 the Chloroplast ATP Synthase Has Distinct Mechanisms and Functions. *Journal of Biological*
1149 *Chemistry* **288**: 13156–13163.

1150 **Kohzuma K, Froehlich JE, Davis GA, Temple JA, Minhas D, Dhingra A, Cruz JA, Kramer DM**. **2017**.
1151 The Role of Light-Dark Regulation of the Chloroplast ATP Synthase. *Frontiers in Plant Science* **8**: 1248.

1152 **Konno H, Nakane T, Yoshida M, Ueoka-Nakanishi H, Hara S, Hisabori T**. **2012**. Thiol Modulation of
1153 the Chloroplast ATP Synthase is Dependent on the Energization of Thylakoid Membranes. *Plant and*
1154 *Cell Physiology* **53**: 626–634.

1155 **Kozakov D, Hall DR, Xia B, Porter KA, Padhorny D, Yueh C, Beglov D, Vajda S**. **2017**. The ClusPro web
1156 server for protein–protein docking. *Nature Protocols* **12**: 255–278.

1157 **Kramer DM, Crofts AR**. **1989**. Activation of the Chloroplast Atpase Measured by the Electrochromic
1158 Change in Leaves of Intact Plants. *Biochimica et biophysica acta* **976**: 28–41.

1159 **Kramer M, Rodriguez-Heredia M, Saccon F, Mosebach L, Twachtmann M, Krieger-Liszkay A, Duffy**
1160 **C, Knell RJ, Finazzi G, Hanke GT**. **2021**. Regulation of photosynthetic electron flow on dark to light
1161 transition by ferredoxin:NADP(H) oxidoreductase interactions. *eLife* **10**.

1162 **Kramer DM, Wise RR, Frederick JR, Alm DM, Hesketh JD, Ort DR, Crofts AR**. **1990**. Regulation of
1163 Coupling Factor in Field-Grown Sunflower - a Redox Model Relating Coupling Factor Activity to the
1164 Activities of Other Thioredoxin-Dependent Chloroplast Enzymes. *Photosynthesis Research* **26**: 213–
1165 222.

1166 **Krishnan-Schmieden M, Konold PE, Kennis JTM, Pandit A**. **2021**. The molecular pH-response
1167 mechanism of the plant light-stress sensor PsbS. *Nature Communications* **12**: 2291.

1168 **Lepistö A, Kangasjärvi S, Luomala E-M, Brader G, Sipari N, Keränen M, Keinänen M, Rintamäki E**.
1169 **2009**. Chloroplast NADPH-Thioredoxin Reductase Interacts with Photoperiodic Development in
1170 Arabidopsis. *Plant Physiology* **149**: 1261–1276.

1171 **Lima-Melo Y, Gollan PJ, Tikkanen M, Silveira JAG, Aro E-M**. **2018**. Consequences of photosystem-I
1172 damage and repair on photosynthesis and carbon use in Arabidopsis thaliana. *The Plant Journal* **0**.

1173 **Lindahl M, Florencio FJ**. **2003**. Thioredoxin-linked processes in cyanobacteria are as numerous as in
1174 chloroplasts, but targets are different. *Proceedings of the National Academy of Sciences* **100**: 16107–
1175 16112.

1176 **Llobell A, Fernandez VM, Lopezbarea J**. **1986**. Electron-Transfer between Reduced Methyl Viologen
1177 and Oxidized Glutathione - a New Assay of Saccharomyces-Cerevisiae Glutathione-Reductase.
1178 *Archives of Biochemistry and Biophysics* **250**: 373–381.

1179 **Maekawa S, Ohnishi M, Wada S, Ifuku K, Miyake C**. **2024**. Enhanced Reduction of Ferredoxin in
1180 PGR5-Deficient Mutant of Arabidopsis thaliana Stimulated Ferredoxin-Dependent Cyclic Electron
1181 Flow around Photosystem I. *International Journal of Molecular Sciences* **25**: 2677.

1182 **Margulis K, Zer H, Lis H, Schoffman H, Murik O, Shimakawa G, Krieger-Liszkay A, Keren N**. **2020**.
1183 Over Expression of the Cyanobacterial Pgr5-Homologue Leads to Pseudoreversion in a Gene Coding
1184 for a Putative Esterase in Synechocystis 6803. *Life* **10**: 174.

1185 **Mathiot C, Alric J**. **2021**. Standard units for ElectroChromic Shift measurements in plant biology.
1186 *Journal of Experimental Botany* **72**: 6467–6473.

1187 **McCarty RE, Fagan J**. **1973**. Light-stimulated incorporation of N-ethylmaleimide into coupling factor
1188 1 in spinach chloroplasts. *Biochemistry* **12**: 1503–1507.

1189 **McKinney DW, Buchanan BB, Wolosiuk RA**. **1978**. Activation of Chloroplast Atpase by Reduced
1190 Thioredoxin. *Phytochemistry* **17**: 794–795.

1191 **Meng EC, Goddard TD, Pettersen EF, Couch GS, Pearson ZJ, Morris JH, Ferrin TE**. **2023**. <scp>UCSF
1192 ChimeraX</scp>: Tools for structure building and analysis. *Protein Science* **32**.

1193 **Miller NT, Vaughn MD, Burnap RL**. **2021**. Electron flow through NDH-1 complexes is the major driver
1194 of cyclic electron flow-dependent proton pumping in cyanobacteria. *Biochimica et Biophysica Acta*
1195 *(BBA) - Bioenergetics* **1862**: 148354.

1196 **Mirdita M, Schütze K, Moriwaki Y, Heo L, Ovchinnikov S, Steinegger M**. **2022**. ColabFold: making
1197 protein folding accessible to all. *Nature Methods* **19**: 679–682.

1198 **Moore V, Vermaas W**. **2024**. Functional consequences of modification of the photosystem
1199 I/photosystem II ratio in the cyanobacterium *Synechocystis* sp. PCC 6803. *Journal of Bacteriology*
1200 **206**.

1201 **Mosebach L, Heilmann C, Mutoh R, Gäbelein P, Steinbeck J, Happe T, Ikegami T, Hanke G, Kurisu G,**
1202 **Hippler M**. **2017**. Association of Ferredoxin:NADP(+) oxidoreductase with the photosynthetic

1203 apparatus modulates electron transfer in Chlamydomonas reinhardtii. *Photosynthesis Research* **134**:
1204 291–306.

1205 **Munekage Y, Hojo M, Meurer J, Endo T, Tasaka M, Shikanai T**. **2002**. PGR5 is involved in cyclic
1206 electron flow around photosystem I and is essential for photoprotection in Arabidopsis. *Cell* **110**:
1207 361–371.

1208 **Murakami S, Kondo K, Katayama S, Hara S, Sunamura E, Yamashita E, Groth G, Hisabori T**. **2018**.
1209 Structure of the γ–ε complex of cyanobacterial F1-ATPase reveals a suppression mechanism of the γ
1210 subunit on ATP hydrolysis in phototrophs. *Biochemical Journal* **475**: 2925–2939.

1211 **Mustila H, Paananen P, Battchikova N, Santana-Sanchez A, Muth-Pawlak D, Hagemann M, Aro E-**
1212 **M, Allahverdiyeva Y**. **2016**. The Flavodiiron Protein Flv3 Functions as a Homo-Oligomer During Stress
1213 Acclimation and is Distinct from the Flv1/Flv3 Hetero-Oligomer Specific to the O-2 Photoreduction
1214 Pathway. *Plant and Cell Physiology* **57**: 1468–1483.

1215 **Nalin CM, McCarty RE**. **1984**. Role of a Disulfide Bond in the Gamma-Subunit in Activation of the
1216 Atpase of Chloroplast Coupling Factor-i. *Journal of Biological Chemistry* **259**: 7275–7280.

1217 **Nandha B, Finazzi G, Joliot P, Hald S, Johnson GN**. **2007**. The role of PGR5 in the redox poising of
1218 photosynthetic electron transport. *Biochimica et Biophysica Acta (BBA) - Bioenergetics* **1767**: 1252–
1219 1259.

1220 **Naranjo B, Penzler J-F, Rühle T, Leister D**. **2021**. NTRC Effects on Non-Photochemical Quenching
1221 Depends on PGR5. *Antioxidants* **10**: 900.

1222 **Nikkanen L, Guinea Diaz M, Toivola J, Tiwari A, Rintamäki E**. **2019**. Multilevel regulation of non-
1223 photochemical quenching and state transitions by chloroplast NADPH-dependent thioredoxin
1224 reductase. *Physiologia Plantarum* **166**.

1225 **Nikkanen L, Santana Sánchez A, Ermakova M, Rögner M, Cournac L, Allahverdiyeva Y**. **2020**.
1226 Functional redundancy between flavodiiron proteins and NDH-1 in Synechocystis sp. PCC 6803. *The*
1227 *Plant Journal: for cell and molecular biology* **103**: 1460–1476.

1228 **Nikkanen L, Solymosi D, Jokel M, Allahverdiyeva Y**. **2021**. Regulatory electron transport pathways of
1229 photosynthesis in cyanobacteria and microalgae: Recent advances and biotechnological prospects.
1230 *Physiologia Plantarum* **173**: 514–525.

1231 **Nikkanen L, Toivola J, Rintamäki E**. **2016**. Crosstalk between chloroplast thioredoxin systems in
1232 regulation of photosynthesis. *Plant Cell and Environment* **39**: 1691–1705.

1233 **Nikkanen L, Toivola J, Trotta A, Guinea Diaz M, Tikkanen M, Aro E-M, Rintamäki E**. **2018**.
1234 Regulation of cyclic electron flow by chloroplast NADPH-dependent thioredoxin system. *Plant Direct*
1235 **2**: 1–24.

1236 **Nikkanen L, Vakal S, Hubáček M, Santana-Sánchez A, Konert G, Wang Y, Boehm M, Gutekunst K,**
1237 **Salminen TA, Allahverdiyeva Y**. **2025**. Flavodiiron proteins associate pH-dependently with the
1238 thylakoid membrane for ferredoxin-1-powered O2 photoreduction. *New Phytologist*.

1239 **Nishikawa Y, Yamamoto H, Okegawa Y, Wada S, Sato N, Taira Y, Sugimoto K, Makino A, Shikanai T**.
1240 **2012**. PGR5-Dependent Cyclic Electron Transport Around PSI Contributes to the Redox Homeostasis
1241 in Chloroplasts Rather Than CO2 Fixation and Biomass Production in Rice. *Plant and Cell Physiology*
1242 **53**: 2117–2126.

1243 **Nix SJ, Morton CJ, Furbank RT, Ermakova M**. **2024**. A novel *PGRL1* paralog refined the control of
1244 photoprotection in grasses and facilitated cell specialisation in C_4 photosynthesis.

1245 **Niyogi KK, Truong TB**. **2013**. Evolution of flexible non-photochemical quenching mechanisms that
1246 regulate light harvesting in oxygenic photosynthesis. *Current Opinion in Plant Biology* **16**: 307–314.

1247 **Okegawa Y, Motohashi K**. **2020**. M-type thioredoxins regulate the PGR5/PGRL1-dependent pathway
1248 by forming a disulfide-linked complex with PGRL1. *Plant Cell* **32**: 3866–3883.

1249 **Ortega-Martínez P, Nikkanen L, Wey LT, Florencio FJ, Allahverdiyeva Y, Díaz-Troya S**. **2024**.
1250 Glycogen synthesis prevents metabolic imbalance and disruption of photosynthetic electron
1251 transport from photosystem <scp>II</scp> during transition to photomixotrophy in *Synechocystis* sp.
1252 <scp>PCC</scp> 6803. *New Phytologist* **243**: 162–179.

1253 **Penzler J-F, Marino G, Reiter B, Kleine T, Naranjo B, Leister D**. **2022**. Commonalities and specialties
1254 in photosynthetic functions of PROTON GRADIENT REGULATION5 variants in Arabidopsis. *Plant*
1255 *Physiology* **190**: 1866–1882.

1256 **Pérez-Ruiz JM, Naranjo B, Ojeda V, Guinea M, Cejudo FJ**. **2017**. NTRC-dependent redox balance of
1257 2-Cys peroxiredoxins is needed for optimal function of the photosynthetic apparatus. *Proceedings of*
1258 *the National Academy of Sciences* **114**: 12069–12074.

1259 **Rantala S, Lempiäinen T, Gerotto C, Tiwari A, Aro EM, Tikkanen M**. **2020**. PGR5 and NDH-1 systems
1260 do not function as protective electron acceptors but mitigate the consequences of PSI inhibition.
1261 *Biochimica et Biophysica Acta - Bioenergetics* **1861**.

1262 **Rey P, Henri P, Alric J, Blanchard L, Viola S**. **2024**. Participation of the stress-responsive CDSP32
1263 thioredoxin in the modulation of chloroplast ATP-synthase activity in *Solanum tuberosum*. *Plant, Cell*
1264 *& Environment*.

1265 **Richter ML, McCarty RE**. **1987**. Energy-dependent changes in the conformation of the epsilon
1266 subunit of the chloroplast ATP synthase. *Journal of Biological Chemistry* **262**: 15037–15040.

1267 **del Riego G, Casano LM, Martin M, Sabater B**. **2006**. Multiple phosphorylation sites in the beta
1268 subunit of thylakoid ATP synthase. *Photosynthesis Research* **89**: 11–18.

1269 **Rühle T, Dann M, Reiter B, Schünemann D, Naranjo B, Penzler J-F, Kleine T, Leister D**. **2021**. PGRL2
1270 triggers degradation of PGR5 in the absence of PGRL1. *Nature Communications* **12**: 3941.

1271 **Sacksteder CA, Kramer DM**. **2000**. Dark-interval relaxation kinetics (DIRK) of absorbance changes as
1272 a quantitative probe of steady-state electron transfer. *Photosynthesis Research* **66**: 145–158.

1273 **Santana-Sánchez A, Nikkanen L, Werner E, Tóth G, Ermakova M, Kosourov S, Walter J, He M, Aro E,**
1274 **Allahverdiyeva Y**. **2023**. Flv3A facilitates O2 photoreduction and affects H2 photoproduction
1275 independently of Flv1A in diazotrophic Anabaena filaments. *New Phytologist* **237**: 126–139.

1276 **Santana-Sanchez A, Solymosi D, Mustila H, Bersanini L, Aro E-M, Allahverdiyeva Y**. **2019**.
1277 Flavodiiron proteins 1-to-4 function in versatile combinations in O-2 photoreduction in
1278 cyanobacteria. *Elife* **8**: e45766.

1279 **Schreiber U, Klughammer C**. **2008**. New accessory for the DUAL-PAM-100: The P515/535 module
1280 and examples of its application. *PAM Application Notes* **1**: 1–10.

1281 **Schreiber U, Klughammer C, Walz H**. **2008**. *Complementary PS II quantum yields calculated from*
1282 *simple fluorescence parameters measured by PAM fluorometry and the Saturation Pulse method*.

1283 **Schwarz O, Schürmann P, Strotmann H**. **1997**. Kinetics and thioredoxin specificity of thiol
1284 modulation of the chloroplast H+-ATPase. *Journal of Biological Chemistry* **272**: 16924–16927.

1285 **Sehnal D, Bittrich S, Deshpande M, Svobodová R, Berka K, Bazgier V, Velankar S, Burley SK, Koča J,**
1286 **Rose AS**. **2021**. Mol* Viewer: modern web app for 3D visualization and analysis of large biomolecular
1287 structures. *Nucleic Acids Research* **49**: W431–W437.

1288 **Sekiguchi T, Yoshida K, Okegawa Y, Motohashi K, Wakabayashi K, Hisabori T**. **2020**. Chloroplast ATP
1289 synthase is reduced by both f-type and m-type thioredoxins. *Biochimica et Biophysica Acta (BBA) -*
1290 *Bioenergetics* **1861**: 148261.

1291 **Sekiguchi T, Yoshida K, Wakabayashi K-I, Hisabori T**. **2022**. Dissipation of the proton electrochemical
1292 gradient in chloroplasts promotes the oxidation of ATP synthase by thioredoxin-like proteins. *Journal*
1293 *of Biological Chemistry* **298**: 102541.

1294 **Sekiguchi T, Yoshida K, Wakabayashi K, Hisabori T**. **2024**. Proton gradient across the chloroplast
1295 thylakoid membrane governs the redox regulatory function of ATP synthase. *Journal of Biological*
1296 *Chemistry* **300**: 107659.

1297 **Sétif P**. **2015**. Electron-transfer kinetics in cyanobacterial cells: Methyl viologen is a poor inhibitor of
1298 linear electron flow. *Biochimica et Biophysica Acta (BBA) - Bioenergetics* **1847**: 212–222.

1299 **Shapiguzov A, Nikkanen L, Fitzpatrick D, Vainonen JP, Gossens R, Alseekh S, Aarabi F, Tiwari A,**
1300 **Blokhina O, Panzarová K, *et al.* 2020**. Dissecting the interaction of photosynthetic electron transfer
1301 with mitochondrial signalling and hypoxic response in the Arabidopsis rcd1 mutant. *Philosophical*
1302 *Transactions of the Royal Society B: Biological Sciences* **375**.

1303 **Shapiguzov A, Vainonen JP, Hunter K, Tossavainen H, Tiwari A, Järvi S, Hellman M, Aarabi F,**
1304 **Alseekh S, Wybouw B, *et al.* 2019**. Arabidopsis RCD1 coordinates chloroplast and mitochondrial
1305 functions through interaction with ANAC transcription factors. *eLife* **8**.

1306 **Shimakawa G, Shaku K, Miyake C**. **2016**. Oxidation of P700 in Photosystem I Is Essential for the
1307 Growth of Cyanobacteria. *Plant Physiology* **172**: 1443–1450.

1308 **Solymosi D, Nikkanen L, Muth-Pawlak D, Fitzpatrick D, Vasudevan R, Howe CJ, Lea-Smith DJ,**
1309 **Allahverdiyeva Y**. **2020**. Cytochrome cM decreases photosynthesis under photomixotrophy in
1310 synechocystis sp. PCC 6803. *Plant Physiology* **183**.

1311 **Song K, Baumgartner D, Hagemann M, Muro-Pastor AM, Maaß S, Becher D, Hess WR**. **2022**. AtpΘ is
1312 an inhibitor of F0F1 ATP synthase to arrest ATP hydrolysis during low-energy conditions in
1313 cyanobacteria. *Current Biology* **32**: 136-148.e5.

1314 **Soteropoulos P, Ong AM, McCarty RE**. **1994**. Alkylation of cysteine 89 of the gamma subunit of
1315 chloroplast coupling factor 1 with N-ethylmaleimide alters nucleotide interactions. *Journal of*
1316 *Biological Chemistry* **269**: 19810–19816.

1317 **Spetea C, Herdean A, Allorent G, Carraretto L, Finazzi G, Szabo I**. **2017**. An update on the regulation
1318 of photosynthesis by thylakoid ion channels and transporters in Arabidopsis. *Physiologia Plantarum*
1319 **161**: 16–27.

1320 **Sunamura E-I, Konno H, Imashimizu-Kobayashi M, Sugano Y, Hisabori T**. **2010**. Physiological Impact
1321 of Intrinsic ADP Inhibition of Cyanobacterial FoF1 Conferred by the Inherent Sequence Inserted into
1322 the γ Subunit. *Plant and Cell Physiology* **51**: 855–865.

1323 **Suorsa M, Jarvi S, Grieco M, Nurmi M, Pietrzykowska M, Rantala M, Kangasjarvi S, Paakkarinen V,**
1324 **Tikkanen M, Jansson S, *et al.* 2012**. PROTON GRADIENT REGULATION5 Is Essential for Proper
1325 Acclimation of Arabidopsis Photosystem I to Naturally and Artificially Fluctuating Light Conditions.
1326 *Plant Cell* **24**: 2934–2948.

1327 **Takagi D, Amako K, Hashiguchi M, Fukaki H, Ishizaki K, Goh T, Fukao Y, Sano R, Kurata T, Demura T,**
1328 ***et al.* 2017**. Chloroplastic ATP synthase builds up a proton motive force preventing production of
1329 reactive oxygen species in photosystem I. *Plant Journal* **91**: 306–324.

1330 **Takagi D, Miyake C**. **2018**. PROTON GRADIENT REGULATION 5 supports linear electron flow to
1331 oxidize photosystem I. *Physiologia Plantarum* **164**: 337–348.

1332 **Theune ML, Hildebrandt S, Steffen-Heins A, Bilger W, Gutekunst K, Appel J**. **2021**. In-vivo
1333 quantification of electron flow through photosystem I – Cyclic electron transport makes up about
1334 35% in a cyanobacterium. *Biochimica et Biophysica Acta (BBA) - Bioenergetics* **1862**: 148353.

1335 **Tikhonov AN, Khomutov GB, Ruuge EK, Blumenfeld LA**. **1981**. Electron transport control in
1336 chloroplasts. Effects of photosynthetic control monitored by the intrathylakoid pH. *Biochimica et*
1337 *Biophysica Acta (BBA) - Bioenergetics* **637**: 321–333.

1338 **Tikkanen M, Aro EM**. **2014**. Integrative regulatory network of plant thylakoid energy transduction.
1339 *Trends in plant science* **19**: 10–17.

1340 **Tikkanen M, Grieco M, Kangasjarvi S, Aro E-M**. **2010**. Thylakoid Protein Phosphorylation in Higher
1341 Plant Chloroplasts Optimizes Electron Transfer under Fluctuating Light. *Plant Physiology* **152**: 723–
1342 735.

1343 **Tikkanen M, Rantala S, Aro E-M**. **2015**. Electron flow from PSII to PSI under high light is controlled by
1344 PGR5 but not by PSBS. *Frontiers in Plant Science* **6**: 521.

1345 **Tiwari A, Mamedov F, Fitzpatrick D, Gunell S, Tikkanen M, Aro E-M**. **2024**. Differential FeS cluster
1346 photodamage plays a critical role in regulating excess electron flow through photosystem I. *Nature*
1347 *Plants*.

1348 **Tiwari A, Mamedov F, Grieco M, Suorsa M, Jajoo A, Styring S, Tikkanen M, Aro E-M**. **2016**.
1349 Photodamage of iron-sulphur clusters in photosystem I induces non-photochemical energy
1350 dissipation. *Nature Plants* **2**: 16035.

1351 **Vaseghi M-J, Chibani K, Telman W, Liebthal MF, Gerken M, Schnitzer H, Mueller SM, Dietz K-J**.
1352 **2018**. The chloroplast 2-cysteine peroxiredoxin functions as thioredoxin oxidase in redox regulation
1353 of chloroplast metabolism (IT Baldwin, C Foyer, and J-P Reichheld, Eds.). *eLife* **7**: e38194.

1354 **Vialet-Chabrand S, Matthews JSA, Simkin AJ, Raines CA, Lawson T**. **2017**. Importance of
1355 Fluctuations in Light on Plant Photosynthetic Acclimation. *Plant Physiology* **173**: 2163–2179.

1356 **Viola S, Bailleul B, Yu J, Nixon P, Selles J, Joliot P, Wollman F-A**. **2019**. Probing the electric field
1357 across thylakoid membranes in cyanobacteria. *Proceedings of the National Academy of Sciences of*
1358 *the United States of America* **116**: 21900–21906.

1359 **Wada S, Amako K, Miyake C**. **2021**. Identification of a Novel Mutation Exacerbated the PSI
1360 Photoinhibition in pgr5/pgrl1 Mutants; Caution for Overestimation of the Phenotypes in Arabidopsis
1361 pgr5-1 Mutant. *Cells* **10**: 2884.

1362 **Wada S, Yamamoto H, Suzuki Y, Yamori W, Shikanai T, Makino A**. **2018**. Flavodiiron Protein
1363 Substitutes for Cyclic Electron Flow without Competing CO2 Assimilation in Rice. *Plant Physiology*
1364 **176**: 1509–1518.

1365 **Wang C, Shikanai T**. **2019**. Modification of Activity of the Thylakoid H+/K+ Antiporter KEA3 Disturbs
1366 Delta pH-Dependent Regulation of Photosynthesis. *Plant Physiology* **181**: 762–773.

1367 **Wang C, Takahashi H, Shikanai T**. **2018**. PROTON GRADIENT REGULATION 5 contributes to
1368 ferredoxin-dependent cyclic phosphorylation in ruptured chloroplasts. *Biochimica Et Biophysica*
1369 *Acta-Bioenergetics* **1859**: 1173–1179.

1370 **Wang C, Yamamoto H, Shikanai T**. **2015**. Role of cyclic electron transport around photosystem I in
1371 regulating proton motive force. *Biochimica Et Biophysica Acta-Bioenergetics* **1847**: 931–938.

1372 **Wolf B, Isaacson T, Tiwari V, Dangoor I, Mufkadi S, Danon A**. **2020**. Redox regulation of PGRL1 at
1373 the onset of low light intensity. *The Plant Journal* **103**: 715–725.

1374 **Woodford R, Watkins J, Moore M, Nix SJ, Yee S, Chan KX, Pogson BJ, von Caemmerer S, Furbank**
1375 **RT, Ermakova M**. **2024**. PGR5 promotes energy-dependent non-photochemical quenching to enable
1376 efficient C4 photosynthesis under fluctuating light. *bioRxiv*: 2024.09.15.613160.

1377 **Wu X, Wu J, Wang Y, He M, He M, Liu W, Shu S, Sun J, Guo S**. **2021**. The key cyclic electron flow
1378 protein PGR5 associates with cytochrome b6f, and its function is partially influenced by the LHCII
1379 state transition. *Horticulture Research* **8**: 55.

Yamamoto H, Shikanai T. **2019**. PGR5-Dependent Cyclic Electron Flow Protects Photosystem I under Fluctuating Light at Donor and Acceptor Sides. *Plant Physiology*: pp.01343.2018.

Yamamoto H, Shikanai T. **2020**. Does the Arabidopsis *proton gradient regulation5* Mutant Leak Protons from the Thylakoid Membrane? *Plant Physiology* **184**: 421–427.

Yamamoto H, Takahashi S, Badger MR, Shikanai T. **2016**. Artificial remodelling of alternative electron flow by flavodiiron proteins in Arabidopsis. *Nature Plants* **2**: 16012.

Yeremenko N, Jeanjean R, Prommeenate P, Krasikov V, Nixon PJ, Vermaas WFJ, Havaux M, Matthijs HCP. **2005**. Open reading frame ssr2016 is required for antimycin A-sensitive photosystem I-driven cyclic electron flow in the cyanobacterium Synechocystis sp PCC 6803. *Plant and Cell Physiology* **46**: 1433–1436.

Yoshida K, Hara A, Sugiura K, Fukaya Y, Hisabori T. **2018**. Thioredoxin-like2/2-Cys peroxiredoxin redox cascade supports oxidative thiol modulation in chloroplasts. *Proceedings of the National Academy of Sciences* **115**: E8296–E8304.

Zhang P, Allahverdiyeva Y, Eisenhut M, Aro E-M. **2009**. Flavodiiron Proteins in Oxygenic Photosynthetic Organisms: Photoprotection of Photosystem II by Flv2 and Flv4 in Synechocystis sp PCC 6803. *Plos One* **4**: e5331.

Zhou Q, Yamamoto H, Shikanai T. **2023**. Distinct contribution of two cyclic electron transport pathways to P700 oxidation. *Plant Physiology* **192**: 326–341.

Zimmer D, Swart C, Graf A, Arrivault S, Tillich M, Proost S, Nikoloski Z, Stitt M, Bock R, Mühlhaus T, *et al.* 2021. Topology of the redox network during induction of photosynthesis as revealed by time-resolved proteomics in tobacco. *Science Advances* **7**.

Figure Legends

Figure 1. Effect of PGR5 and $CF_1\gamma$ redox state on *pmf*, thylakoid conductivity, and photoprotection in fluctuating light in *Arabidopsis*. (a) Proton conductivity of the thylakoid membrane (g_H+ s^{-1}), **(b)** magnitude of the *pmf*, and **(c)** Thylakoid proton flux ($v_H+ = g_H+ \times pmf$) in fluctuating light, as determined from dark-interval relaxation kinetics (DIRK) of the ECS signal. ECS was measured from dark-adapted WT-gl1 and *pgr5-1* mutant *Arabidopsis* leaves under a light regime alternating between 1 min periods of low (50 µmol photons $m^{-2}s^{-1}$) and high light (825 µmol photons $m^{-2}s^{-1}$). The values in (a) and (c) are averages from 9 and in (b) 11 biological replicates ± SEM. **(d)** Quantum yield of non-photochemical quenching (Y(NPQ)) and **(e)** fraction of oxidised P700 (donor side limitation of PSI, Y(ND)) in a fluctuating light regime supplemented with saturating pulses at 15 s intervals. The values in (d–e) are averages from 3 biological replicates ± SEM. In (a–e) * indicates statistically significant difference between WT and *pgr5-1* according to a two-sample Student's t-test ($P<0.05$). **(f-g)** Mobility shift assays of the *in vivo* thiol redox state of the CF_1y subunit of the

chloroplast ATP synthase in WT (f) and in *pgr5-1* (g). Samples were taken from fluctuating light (1 min periods of 50 µmol photons $m^{-2}s^{-1}$, LL, and 825 µmol photons $m^{-2}s^{-1}$, HL. The break between the 140 and 160 sec samples in (f) represents division between two gels. –DTT indicates control sample where DTT was not added after NEM incubation and no alkylation of thiols by MALPEG should occur.

Figure 2. ***Pmf* dynamics, PSI oxidation, O_2 fluxes, and growth under fluctuating light in *Synechocystis*.** Thylakoid conductivity (g_H+) **(a)**, *pmf* **(b),** and proton flux (vH+) **(c)** were determined by the ECS DIRK method from WT, *Δpgr5, Δpgr5 flv3,* and *Δflv3* cells. The values in a–c are averages from 3–6 (depending on the quality of the first-order DIRK fit) biological replicates ± SEM, apart from the second data points of WT and *Δpgr5*, where signal-to-noise ratio allowed only single replicates to be fitted successfully. * indicates statistically significant differences between WT and *Δpgr5* according to a two-sample Student's t-test (P<0.05). **(d)** Representative ECS decay kinetics in WT and *Δpgr5* cells during the second-to-last 600 ms dark interval in the experiment. First order exponential fits are shown in cyan and turquoise. **(e)** Donor (Y(ND)) and **(f)** acceptor side limitation (Y(NA)) of PSI in WT, Δ*pgr5*, Δ*pgr5 flv3*, and Δ*flv3* strains of *Synechocystis* during transitions from low light (25 µmol photons $m^{-2}s^{-1}$, LL) to high light (525 µmol photons $m^{-2}s^{-1}$, HL). Y(NA) and Y(ND) were determined from P700 redox kinetics using the saturating pulse method on a DUAL-PAM 100 spectrophotometer. Traces are averages of 3–4 biological replicates ± SEM (ribbons). * indicates statistically significant difference to WT according to a two-sample Student's t-test (P<0.05). **(g)** Growth curves (OD 750 nm) of WT, *Δpgr5* and *Δpgr5 flv3* cells under fluctuating light (5 min at 20 µmol photons $m^{-2}s^{-1}$ to 30 sec at 500 µmol photons $m^{-2}s^{-1}$). The values are averages from 3 biological replicates ± SEM. **(h)** Quantification of LET and CET rates in *Synechocystis* WT and Δ*pgr5*. Chlorophyll was adjusted to 20 µg Chl ml^{-1} in BG-11 pH 7.5. Using a Dual KLAS-NIR spectrophotometer, cells were illuminated for 2 min under 500 µmol photons $m^{-2}s^{-1}$ before administering 100x 40 ms dark intervals 10 s apart to monitor the relaxation kinetics of the P700 and PC signals. The measurement was then repeated in the presence of 10µM DCMU to inhibit LET. Values means of four biological replicates ± SD. **(i)** O_2 gas fluxes in fluctuating light in WT and *Δpgr5* as measured by membrane inlet mass spectrometry (MIMS). Cells were grown in fluctuating light (1 min 25 µmol photons $m^{-2}s^{-1}$ / 1 min 500 µmol photons $m^{-2}s^{-1}$), adjusted to 10 µg Chl ml^{-1}, and $^{18}O_2$ was added in equilibrium with $^{16}O_2$ in order to distinguish O_2 uptake from O_2 evolution. Cells were dark-adapted for 10 min, after which real-time gas fluxes were measured by MIMS mimicking the fluctuating growth light conditions, with a 5 min dark period on either side of three LL-HL cycles. The values are averages of four biological replicates ± SD. The bar chart shows the maximum O_2 uptake rates + SD during the first HL phase of the experiment (dotted arrow). * Indicates statistically significant difference between WT and Δ*pgr5* according to a two-sample Student's t-test (P<0.05).

Figure 3. *Pmf* dynamics in *Chlamydomonas reinhardtii* under fluctuating light. (a) Thylakoid conductivity (g_H+). **(b)** *pmf* ($\Delta ECS/ECS_{ST}$). **(c)** Proton flux (v_H+). The ECS signal was measured from WT137c, *pgr5* knockout mutant, and PGR5 complementation line (PGR5C) cells under a fluctuating light regime, alternating between 1 min periods of low light (50 µmol photons $m^{-2}s^{-1}$) and high light 825 (µmol photons $m^{-2}s^{-1}$). Values are means ± SEM from three biological replicates. The asterisks indicate statistically significant differences between WT and *pgr5* according to a two-sample Student's t-tests (P<0.05).

Figure 4. Correlation of *pmf* with gH+ in WT and PGR5-deficient mutants across photosynthetic organisms. Time-resolved ECS datasets from fluctuating light conditions. **(a)** *Arabidopsis thaliana* dataset from Fig. 1a–c. **(b)** *Arabidopsis thaliana* dataset from Supplementary Fig. S4. **(c)** *Setaria viridis* dataset from Supplementary Fig. S12. **(d)** *Chlamydomonas reinhardtii* dataset from Fig. 3. **(e)** *Synechocystis* sp. PCC 6804 dataset from Fig. 2a–c. (f) *Synechococcus elongatus* sp. PCC 7942 dataset from Supplementary Fig. S11.

Figure 5. Effect of methyl viologen (MV) on thiol redox states of chloroplast enzymes and on regulation of *pmf* in *Arabidopsis*. (a) Mobility shift assays of $AtCF_1y$, 2-CysPrxs, NTRC, and FBPase thiol redox state in vivo. WT Arabidopsis leaves were incubated in H_2O with (+) or without (-) 1 µM MV in dark and then illuminated in GL conditions for 180 min, with samples taken from darkness (0) and after 30, 90, and 180 min of illumination. Total protein extracts were labelled with MALPEG as described in Materials and Methods, separated by SDS-PAGE and probed with appropriate antibodies. MALPEG-labelled (in vivo oxidised) forms migrate more slowly than unlabelled forms (in vivo reduced). –DTT indicates control sample where no alkylation of thiols by MALPEG should occur, and * indicates dimeric 2CysPrx. We cannot fully exclude the possibility of the apparent reduction of chloroplast enzymes in presence of MV being caused by overoxidation of thiols to sulphenic acids (Huang et al., 2019), especially in the case of 2-CysPrxs (Puerto-Galan et al., 2013; Cerveau et al., 2016). S-sulphenylated proteins cannot form disulphides and thus cannot be labelled by the alkylating agent in our protocol, migrating similarly to fully reduced proteins in mobility shift assays. Apart from 2-CysPrxs, where the thiols are required for the catalytic activity of the enzyme, overoxidation may in fact result in in a conformation that is functionally similar to the reduced state of the protein. **(b)** Conductivity of the thylakoid membrane (g_H+) after 1 s of illumination in growth light (GL, 95 µmol photons $m^{-2}s^{-1}$) in dark-adapted WT and *pgr5* mutant leaves incubated in H_2O with or without 1 µM MV. The values are mean + SD from 4–7 biological replicates. Statistical significance of differences was tested by one-way ANOVA and Tukey's tests

(p<0.05). **(c)** Thylakoid conductivity and **(d)** *pmf* in dark-adapted WT and *pgr5* mutant leaves incubated in H_2O with or without 1 µM MV during 5 min illumination in GL (95 µmol photons $m^{-2}s^{-1}$) and consequent increase in light intensity to 825 µmol photons $m^{-2}s^{-1}$ (HL), as determined from dark-interval relaxation kinetics of the ECS signal. The values in C-D are averages from 4–7 biological replicates ± SEM (ribbon).

Figure 6. Effect of NEM on thylakoid conductivity under illumination. (a) The effect of 0.1 mM NEM on gH+ in *Synechocystis* WT and Δ*pgr5* cells. ECS DIRK were measured 5 seconds after the onset of illumination at 500 µmol photons m^{-2} s^{-1}. The values are averages of 7–11 biological replicates + SD. Statistical significance of differences was tested by one-wayANOVA and Tukey's tests for comparison of means (P<0.05**). (b)** The effect of 0.1 mM NEM on gH+ in *Synechococcus elongatus* sp. PCC 7942 WT cells. ECS DIRK were measured as averaged decay kinetics from 5 dark intervals spaced 5 seconds apart, with the first DIRK being administered 5 seconds after the onset of illumination at 500 µmol photons m^{-2} s^{-1}. The values are averages of 3 biological replicates + SD. n.s. = statistically non-significant difference according to a paired *t*-test (P=0.20). **(c)** gH+ was measured in *Arabidopsis* WT-gl1 and *pgr5* mutant leaves incubated on water or water + 0.1 mM NEM. The water samples are the same as in Figure 1, while the +NEM values are averages of 4 biological replicates ± SEM.

Figure 7. Protein–protein interaction between ATP synthase and PGR5. (a) Bimolecular fluorescence complementation (BiFC) test for protein-protein interaction between Arabidopsis $CF_1\gamma$ fused to an N-terminal fragment of yellow fluorescent protein ($AtCF_1\gamma$:YFP-N) and Arabidopsis PGR5 fused to a C-terminal YFP fragment (AtPGR5:YFP-C) in tobacco leaves. The left panel shows Chlorophyll *a* autofluorescence in purple, the middle panel YFP fluorescence in yellow, and the right panel a merged image of YFP and chlorophyll images. The scale bar is 10 µm. **(b)** Predicted interaction complex of *Spinacia oleracea* $CF_1\gamma$ and CF_1□ (Hahn *et al.*, 2018), and AtPGR5 (PDB identifier Q9SL05) docked using the ClusPro 2.0 protein-protein docking service. The $SoCF_1\gamma$ / $SoCF_1$□ / AtPGR5 with the of the Spinach ATP synthase complex ($SoCF_0CF_1$, PDB identifier 6FKF) superimposed (Hahn *et al.*, 2018). Modelling of electrostatic surface charges of AtPGR5 and the surrounding parts of $SoCF_1$ is shown in the smaller inlet on the right. **(c)** An Alphafold2 Multimer prediction of an interaction complex between *Synechocystis* ATP synthase γ subunit (*sll1327*, green), ATP synthase ε subunit (*slr1330*, yellow), and *Synechocystis* Pgr5 (*ssr2016*, magenta). The top-ranked model with a pTM score of 0.797 and an ipTM score of 0.702 is shown.

Figure 8. Hypothetical model of PGR5-mediated downregulation of ATP synthase activity in plant chloroplasts. A model of an *Arabidopsis thaliana* 2xPGRL1a/2xPGR5/TRXm4 complex was created with the protein–protein docking service ClusPro 2.0, docking monomeric AlphaFold models with the PDB identifiers Q8H112, Q9SL05, and Q9SEU6. An interaction complex of AtPGR5, $AtCF_1\gamma$, and $AtCF_1$ was modelled with AlphaFold3 and overlaid with the from the *Spinacia oleracea* CF_0CF_1 crystal structure (6FKF). **(a)** Under low irradiance when stromal redox regulatory systems are largely oxidised, PGR5 is bound to the PGRL1a/PGR5/TRXm4 complex, possibly held by an intermolecular disulphide bond between the Cys116 residues in the PGRL1a monomers. This allows ATP synthase to maintain high activity, effectively dissipating the proton gradient over the thylakoid membrane**. (b)** Under high irradiance, stromal redox regulatory systems become reduced, resulting in reduction of the PGRL1a-dimer disulphide and release of PGR5 to bind to ATP synthase. This inhibits the activity of ATP synthase, lowering thylakoid conductivity to protons, buildup of high *pmf* and induction of photoprotective mechanisms.

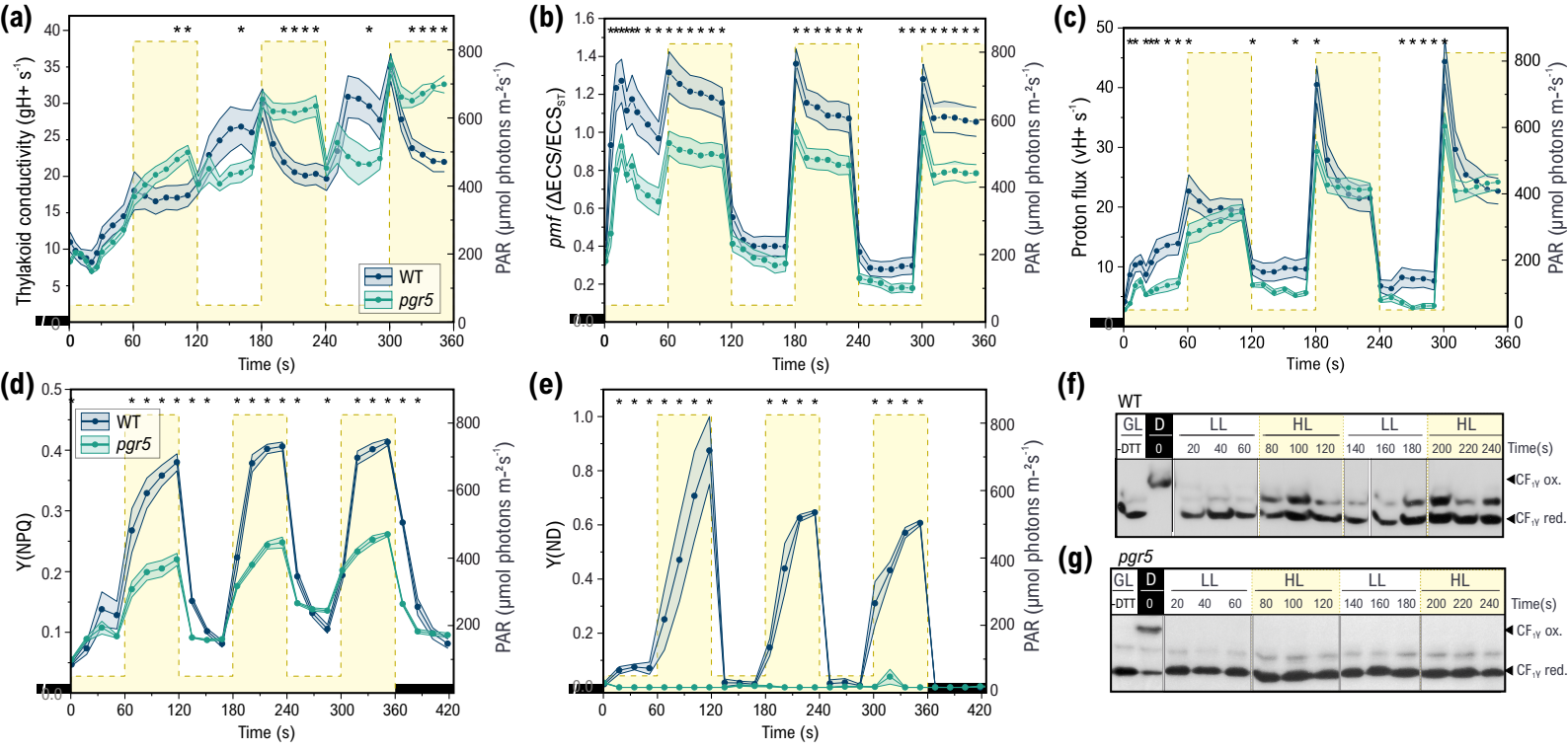
(a)
Thylakoid conductivity (gH+ s-1)
PAR (µmol photons m-2s-1)
Time (s)
WT
pgr5
(b)
pmf (ΔECS/ECSST)
PAR (µmol photons m-2s-1)
Time (s)
(c)
Proton flux (vH+ s-1)
PAR (µmol photons m-2s-1)
Time (s)
(d)
Y(NPQ)
PAR (µmol photons m-2s-1)
Time (s)
WT
pgr5
(e)
Y(ND)
PAR (µmol photons m-2s-1)
Time (s)
(f)
WT
GL
D
LL
HL
LL
HL
-DTT
0
20 40 60 80 100 120 140 160 180 200 220 240
Time(s)
CF1γ ox.
CF1γ red.
(g)
pgr5
GL
D
LL
HL
LL
HL
-DTT
0
20 40 60 80 100 120 140 160 180 200 220 240
Time(s)
CF1γ ox.
CF1γ red.

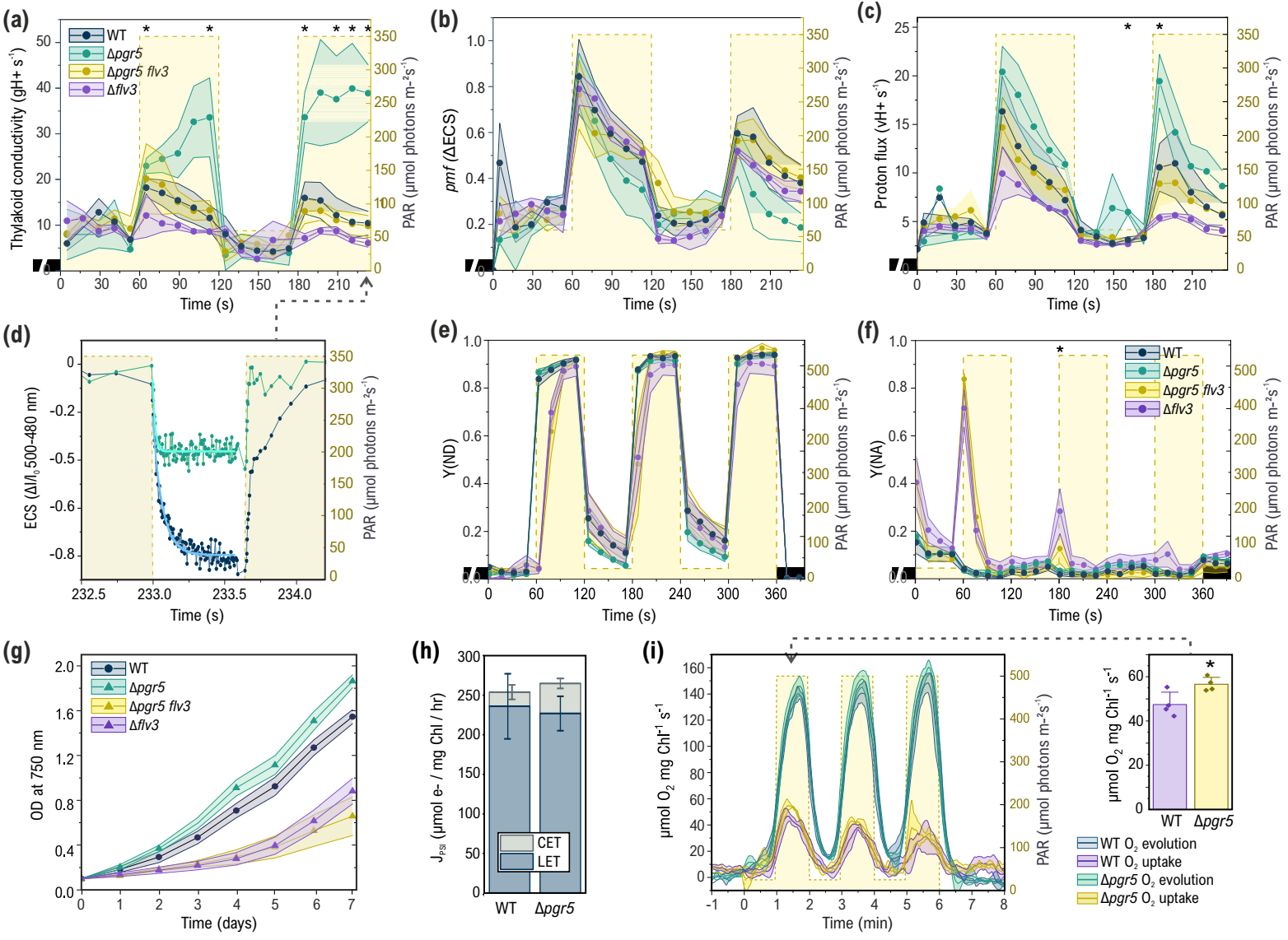
(a)
WT
Δpgr5
Δpgr5 flv3
Δflv3
Thylakoid conductivity (gH+ s-1)
PAR (µmol photons m-2s-1)
Time (s)
(b)
pmf (ΔECS)
PAR (µmol photons m-2s-1)
Time (s)
(c)
Proton flux (vH+ s-1)
PAR (µmol photons m-2s-1)
Time (s)
(d)
ECS (ΔI/I0 500-480 nm)
PAR (µmol photons m-2s-1)
Time (s)
(e)
Y(ND)
PAR (µmol photons m-2s-1)
Time (s)
(f)
Y(NA)
PAR (µmol photons m-2s-1)
Time (s)
(g)
OD at 750 nm
Time (days)
(h)
JPSI (µmol e- / mg Chl / hr)
CET
LET
WT
Δpgr5
(i)
µmol O2 mg Chl-1 s-1
PAR (µmol photons m-2s-1)
Time (min)
µmol O2 mg Chl-1 s-1
WT O2 evolution
WT O2 uptake
Δpgr5 O2 evolution
Δpgr5 O2 uptake

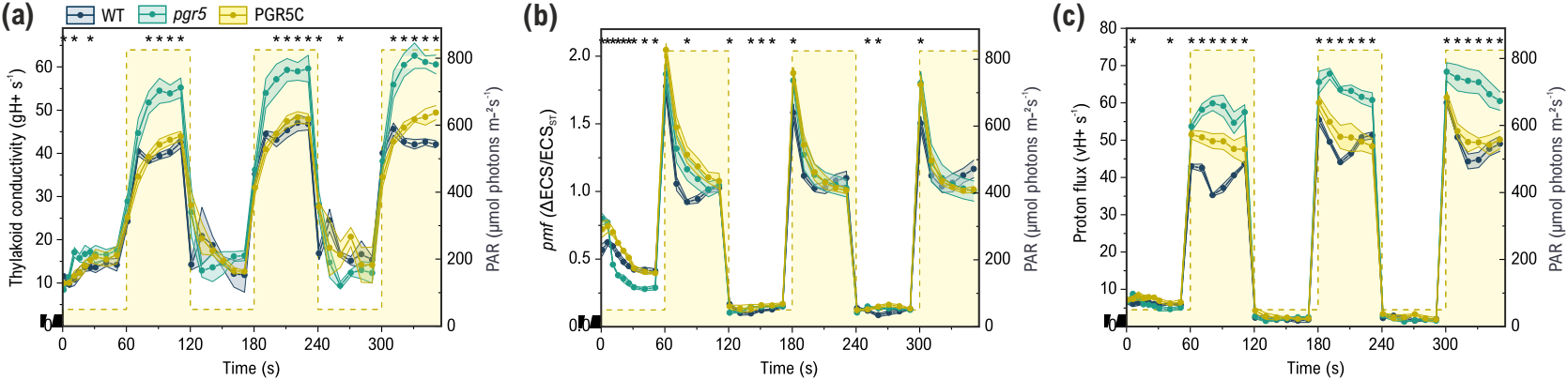
(a)
WT
pgr5
PGR5C
Thylakoid conductivity (gH+ s-1)
PAR (µmol photons m-2s-1)
Time (s)
(b)
pmf (ΔECS/ECSst)
PAR (µmol photons m-2s-1)
Time (s)
(c)
Proton flux (vH+ s-1)
PAR (µmol photons m-2s-1)
Time (s)

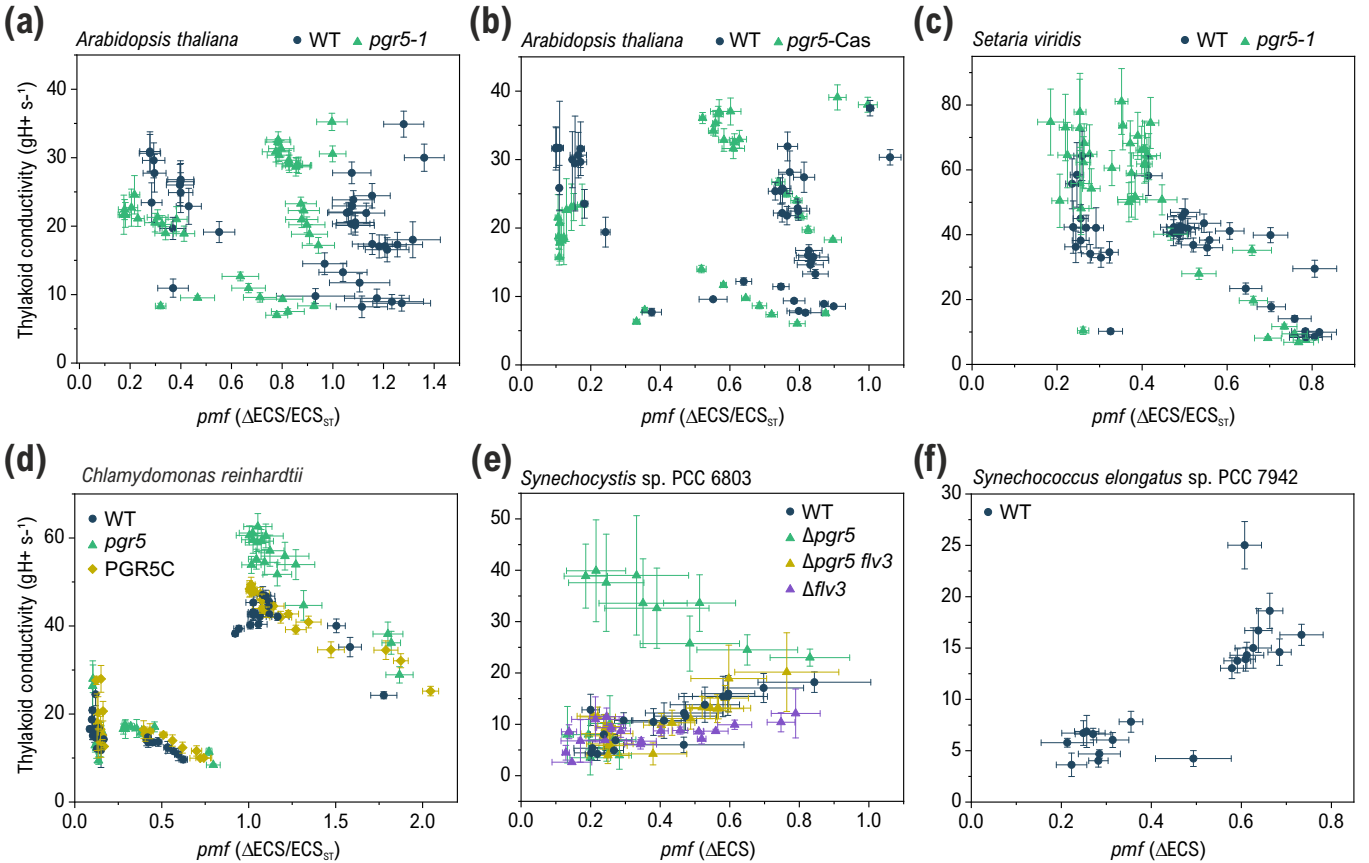
(a)
Arabidopsis thaliana
WT
pgr5-1
Thylakoid conductivity (gH+ s-1)
pmf (ΔECS/ECSST)
(b)
Arabidopsis thaliana
WT
pgr5-Cas
pmf (ΔECS/ECSST)
(c)
Setaria viridis
WT
pgr5-1
pmf (ΔECS/ECSST)
(d)
Chlamydomonas reinhardtii
WT
pgr5
PGR5C
Thylakoid conductivity (gH+ s-1)
pmf (ΔECS/ECSST)
(e)
Synechocystis sp. PCC 6803
WT
Δpgr5
Δpgr5 flv3
Δflv3
pmf (ΔECS)
(f)
Synechococcus elongatus sp. PCC 7942
WT
pmf (ΔECS)

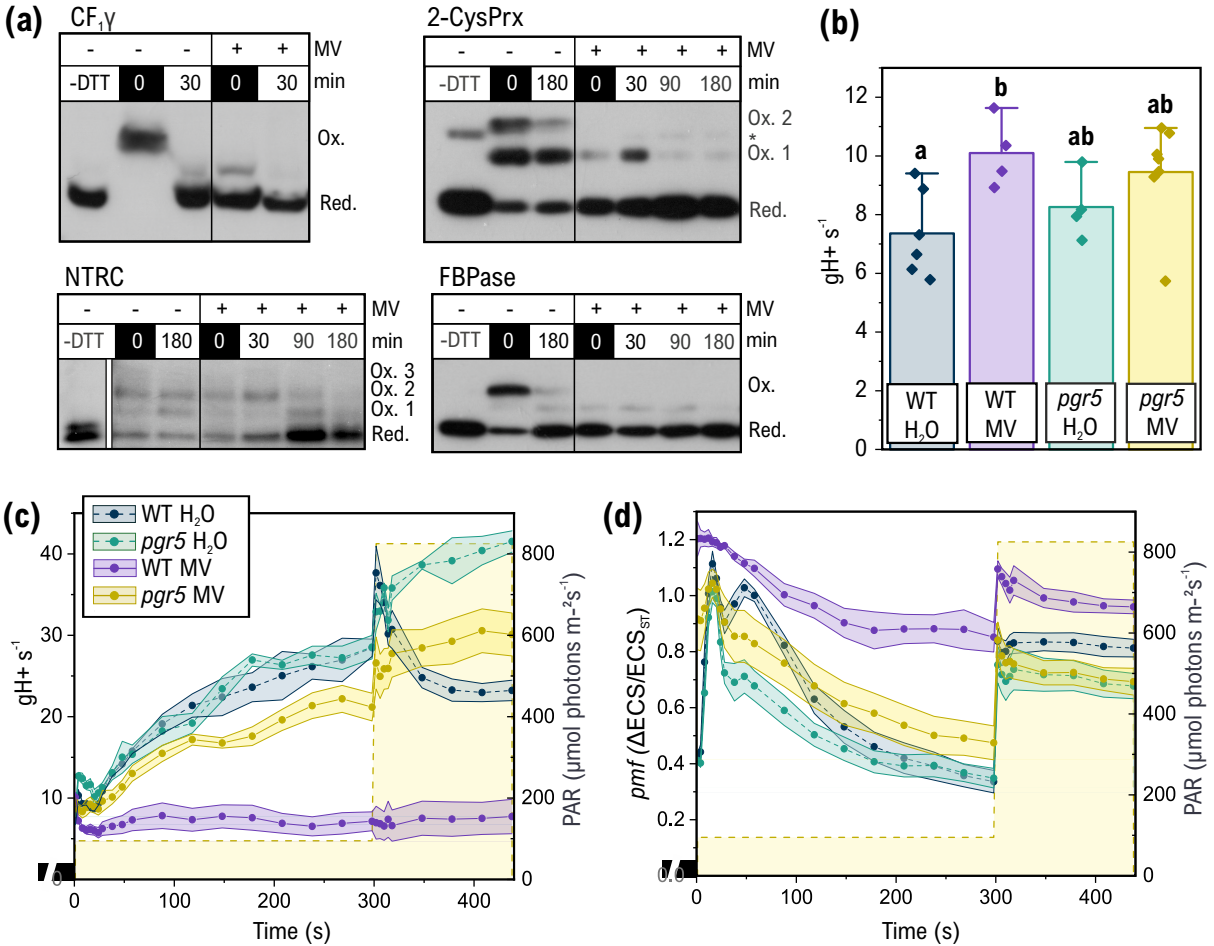
(a)
CF1γ
MV
-DTT
min
Ox.
Red.
2-CysPrx
Ox. 2
Ox. 1
NTRC
Ox. 3
FBPase
(b)
gH+ s-1
a
b
ab
ab
WT H2O
WT MV
pgr5 H2O
pgr5 MV
(c)
WT H2O
pgr5 H2O
WT MV
pgr5 MV
gH+ s-1
PAR (µmol photons m-2s-1)
Time (s)
(d)
pmf (ΔECS/ECSST)
PAR (µmol photons m-2s-1)
Time (s)

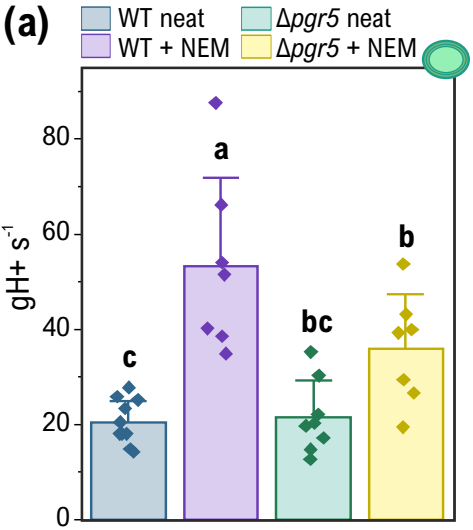
(a)
WT neat
WT + NEM
Δpgr5 neat
Δpgr5 + NEM
gH+ s-1
0
20
40
60
80
c
a
bc
b

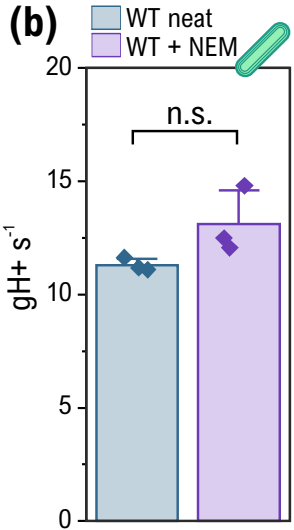
(b)
WT neat
WT + NEM
n.s.
gH+ s-1
0
5
10
15
20

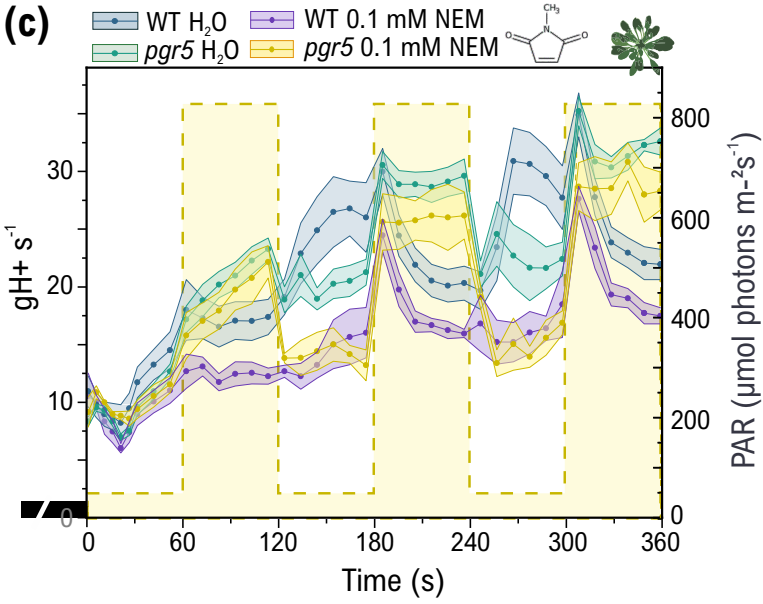
(c)
WT H2O
pgr5 H2O
WT 0.1 mM NEM
pgr5 0.1 mM NEM
gH+ s-1
PAR (µmol photons m-2s-1)
Time (s)
0
60
120
180
240
300
360
10
20
30
200
400
600
800

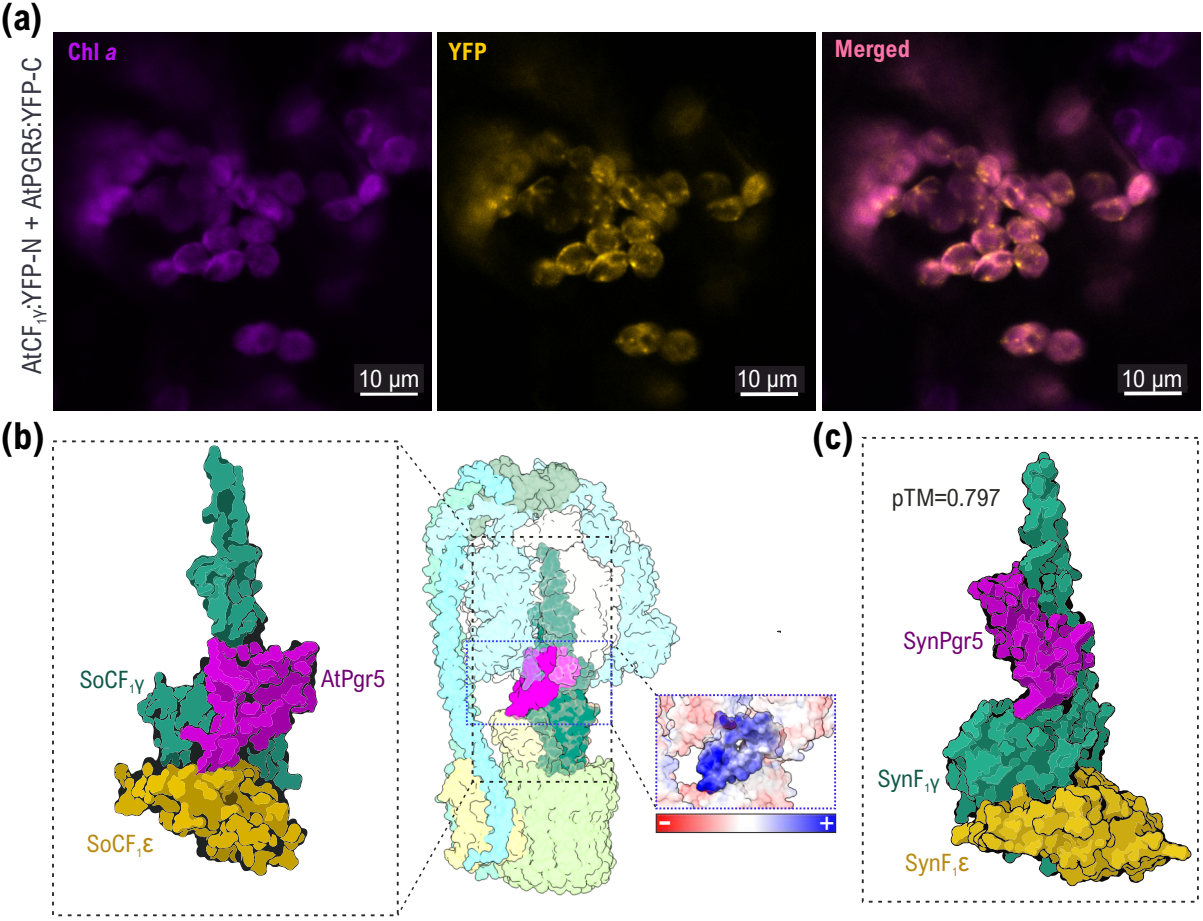
(a)
AtCF1γ:YFP-N + AtPGR5:YFP-C
Chl a
YFP
Merged
10 µm
10 µm
10 µm
(b)
SoCF1γ
AtPgr5
SoCF1ε
(c)
pTM=0.797
SynPgr5
SynF1γ
SynF1ε

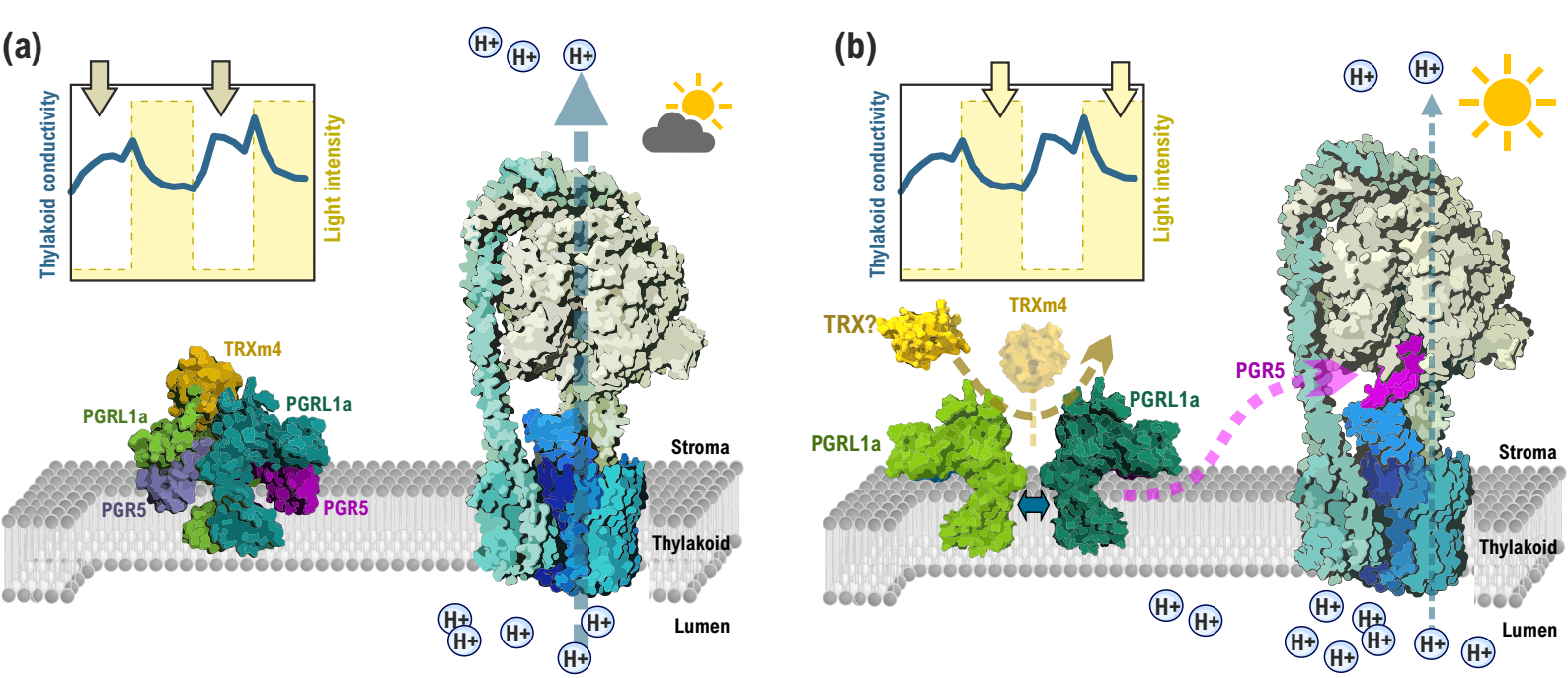
(a)
Thylakoid conductivity
Light intensity
H+
TRXm4
PGRL1a
PGRL1a
PGR5
PGR5
Stroma
Thylakoid
Lumen
(b)
Thylakoid conductivity
Light intensity
TRX?
TRXm4
PGRL1a
PGRL1a
PGR5
Stroma
Thylakoid
Lumen